

General Disclaimer

One or more of the Following Statements may affect this Document

- This document has been reproduced from the best copy furnished by the organizational source. It is being released in the interest of making available as much information as possible.
- This document may contain data, which exceeds the sheet parameters. It was furnished in this condition by the organizational source and is the best copy available.
- This document may contain tone-on-tone or color graphs, charts and/or pictures, which have been reproduced in black and white.
- This document is paginated as submitted by the original source.
- Portions of this document are not fully legible due to the historical nature of some of the material. However, it is the best reproduction available from the original submission.

(NASA-CR-167938) ON FINITE ELEMENT STRESS
ANALYSIS OF SPUR GEARS (Cincinnati Univ.)
53 p HC A04/MF A01 CSCL 131

N82-29607

Unclas

G3/37 28506

NASA Contractor Report 167938

ON FINITE ELEMENT STRESS ANALYSIS OF SPUR GEARS

S. H. Chang and R. L. Huston

University of Cincinnati

Cincinnati, Ohio

July 1982



Prepared for

NATIONAL AERONAUTICS AND SPACE ADMINISTRATION

Lewis Research Center

Under Grant NSG-3188

ORIGINAL PAGE IS
OF POOR QUALITY

INTRODUCTION

This report presents spur gear stress analysis results for a variety of loading conditions, support conditions, root radii and rim thicknesses. These results are obtained by using the SAP IV finite element code [1].*

During the past decade there have been a number of investigations into the nature of spur gear stresses. References [2-13] summarize some of these efforts. They include a variety of theoretical and experimental approaches to determining the stresses, but the results are reasonably consistent. Of particular interest is the fact that the results obtained using finite element techniques are consistent with results obtained using vastly different theoretical and experimental techniques. For example, in 1955, Jacobson [14] studied bending stresses using photoelastic techniques. In 1973, his results were matched by Wilcox and Coleman [12] using finite element techniques. In 1962, Aida and Terauchi [15] studied bending stresses using stress functions and classical elasticity theories, and more recently (1981) Cordou and Tordion [3] studied the stresses using complex variables. Their results also confirm results obtained using finite element techniques. Other noteworthy theoretical studies which confirm finite element results are those of Baronet, Tordion, and Premilhat [2,8] and of Shotter [9].

* Numbers in brackets refer to References at the end of the report.

ORIGINAL PAGE IS
OF POOR QUALITY

Regarding the use of the finite element method itself in gear stress analyses, there have recently been a number of notable achievements. For example, Chabert, Dang Tran, and Mathis [4] have used finite element techniques to examine the stress distribution across the root section. Tobe, Kato and Inoue [10,11], Winter and Hirt [13], Cornell [6], and Wilcox and Coleman [12] have studied root stresses using finite element methods. Finally, Oda, Nagamura, and Aoki have examined the effect of rim thickness on the root stresses using the finite element method.

In this report these results and studies are extended and amplified using the SAP-IV finite element technique [1]. This includes examination of the surface stress distribution for the entire tooth profile for tip and pitch point loading. Also, the root surface stresses and the root section stresses are studied for a variety of loading positions and root radii. Finally, the effect of rim thickness and mounting support upon the root stress is determined.

ANALYSIS

The Model

Figures 1. and 2. show typical finite-element grids used in the analysis. The number of elements used was varied depending upon the particular loading and geometry being considered. Typically the grid had approximately 190 elements and 120 nodes.

The gear tooth itself had a modulus M of 5 (pitch diameter divided by the number of teeth). It was a member of an 18-tooth gear with the pitch diameter thus being 90 mm. The tooth sides are involute curves and the pressure angle was 20° . The root radius and hub thickness were variables. The tooth material was steel with an elastic modulus of $2.11 \times 10^5 \text{ N/mm}^2$.

Loading and Support

The tooth was loaded with a 400 N/mm concentrated line load applied normal to the tooth boundary at various points as shown in Figure 3. The hub or rim was supported alternatively: a) at all points along the boundary, and b) at only the radial points.

The Finite Element Procedure

The SAP-IV finite element code [1] was used to assemble and solve the governing equations

$$Ku = R \quad (1)$$

ORIGINAL PAGE IS
OF POOR QUALITY

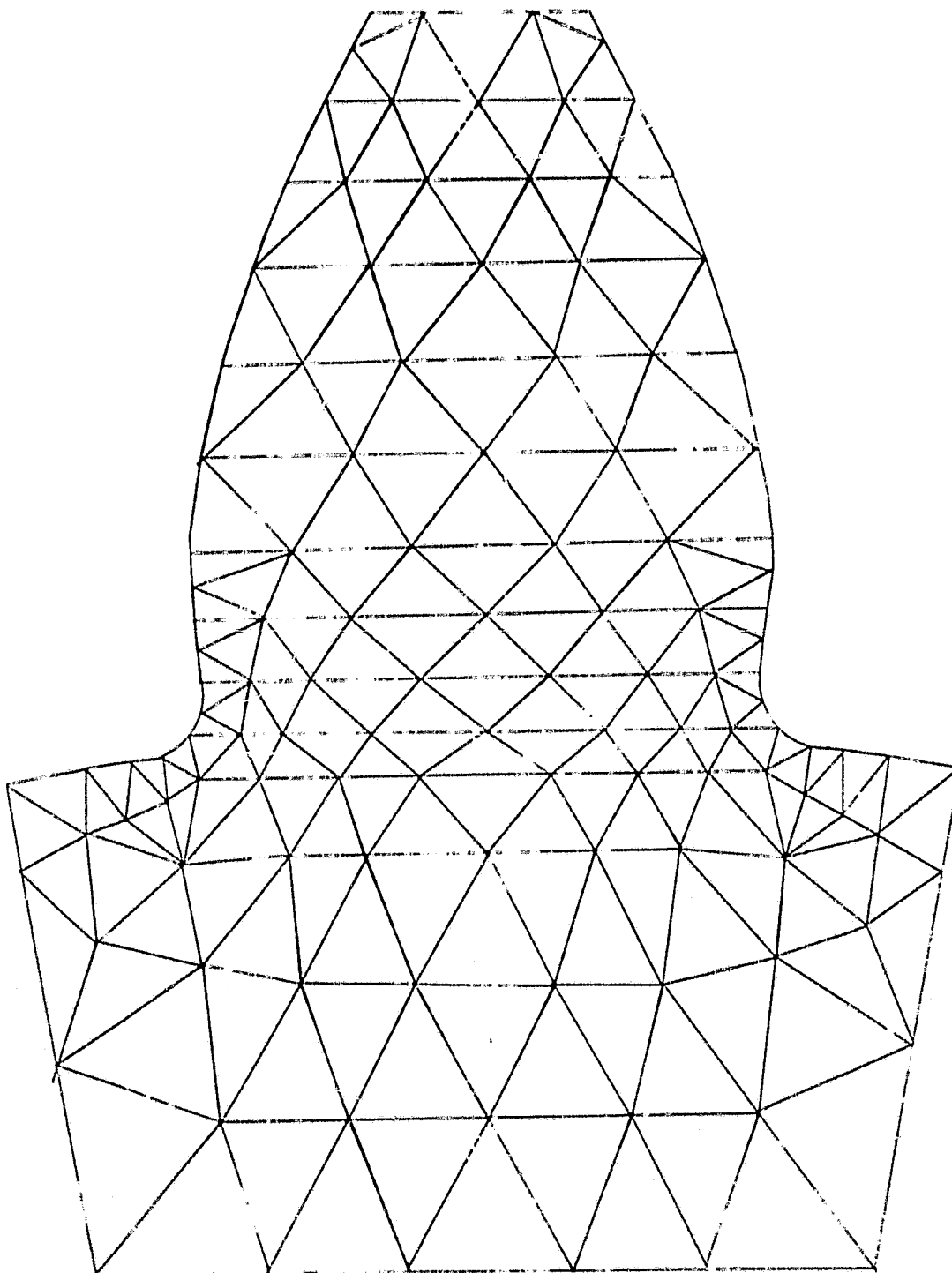


Figure 1. Typical Finite Element Grid (Small Root Radius).

ORIGINAL PAGE IS
OF POOR QUALITY

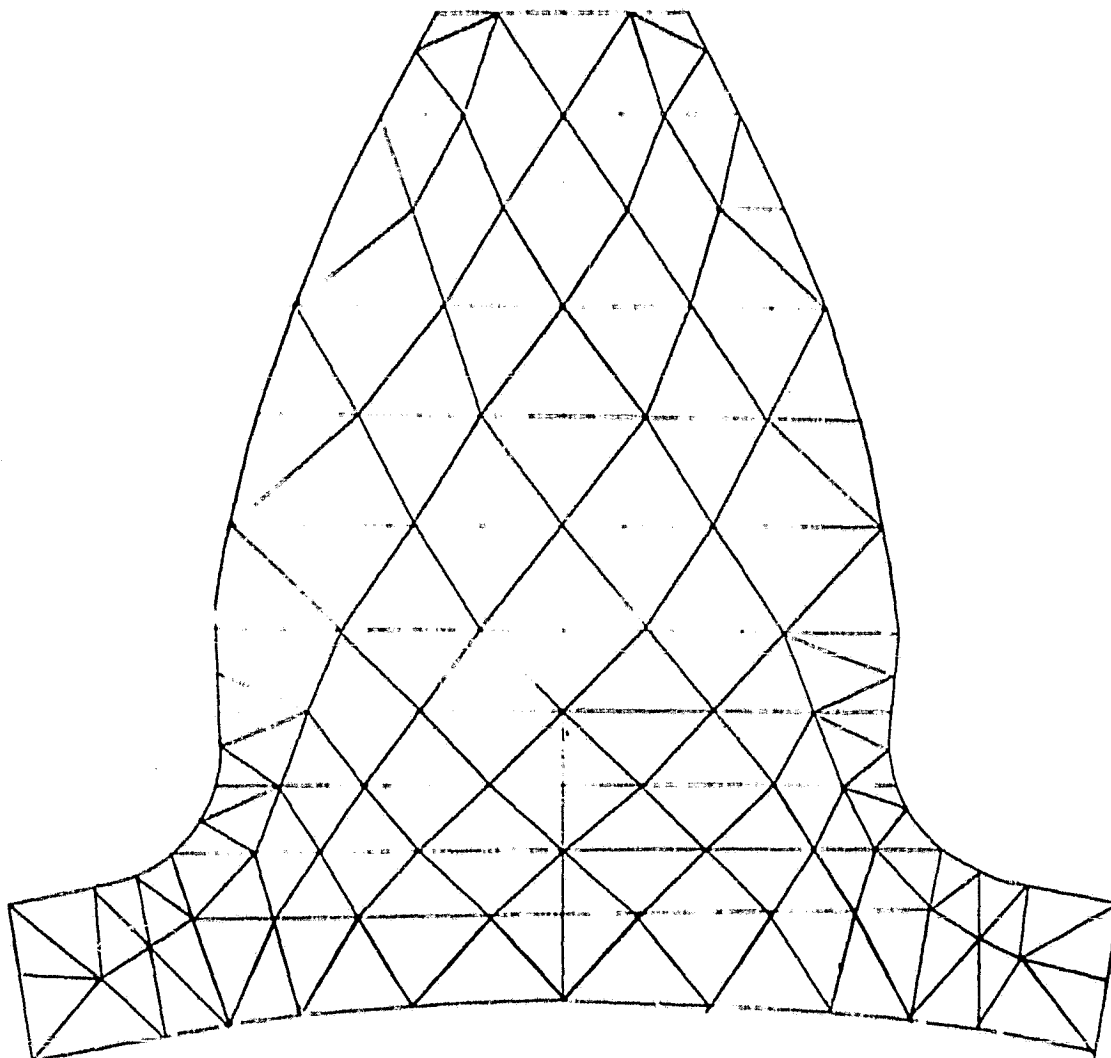


Figure 2. Typical Finite Element Grid (Small Rim Thickness).

where K is the global stiffness matrix, u is the array of nodal displacements, and R is the force array. The solution is obtained using Gauss elimination through the linear equation solver SESOL [1]. After the nodal displacements are found, element stress displacement relations are used to obtain the element stresses.

**ORIGINAL PAGE IS
OF POOR QUALITY**

ORIGINAL PAPER
OF POOR QUALITY

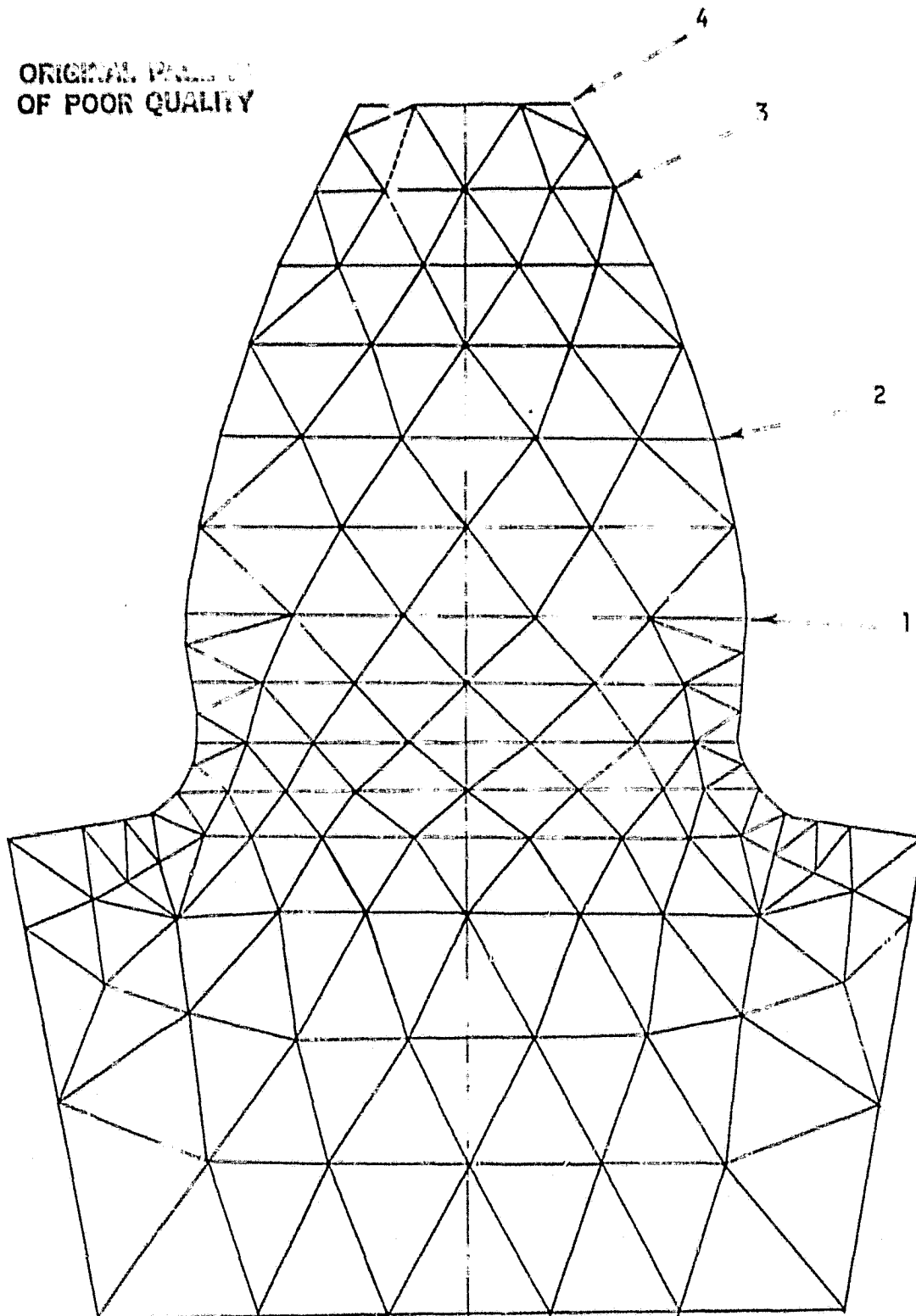


Figure 3. Loading Location for the 400 N/mm Load.

Surface Stress Distribution

First, the stress distribution along the tooth surface was calculated for a tip loading and for a load applied near the pitch point. Figures 4. and 5. contain a representation of the results for the maximum principal surface stress. They show that, except for a local concentration, the maximum stress occurs at the root of the tooth.

Root Surface Stresses as a Function of Root Radius

The above analysis led to a closer examination of the maximum root surface stresses as a function of the root radius. Specifically, the tooth was loaded at the points shown in Figure 3. The root surface stresses were then calculated for radii of 0.2M, 0.3M, and 0.4M or 1.0 mm, 1.5 mm, and 2.0 mm respectively. The results are shown in Figures 6., 7., and 8. An examination of the numerical values associated with these figures shows the stresses increase linearly with the inverse of the root radii, for the range of radii considered. Also, the stresses are seen to increase linearly with the distance from the root to the point of application of the load. These results are consistent with those obtained and recorded by Chabert, et al. [4], and with those of short beam theory as recorded by Roark and Young [16].

ORIGINAL PAGE IS
OF POOR QUALITY

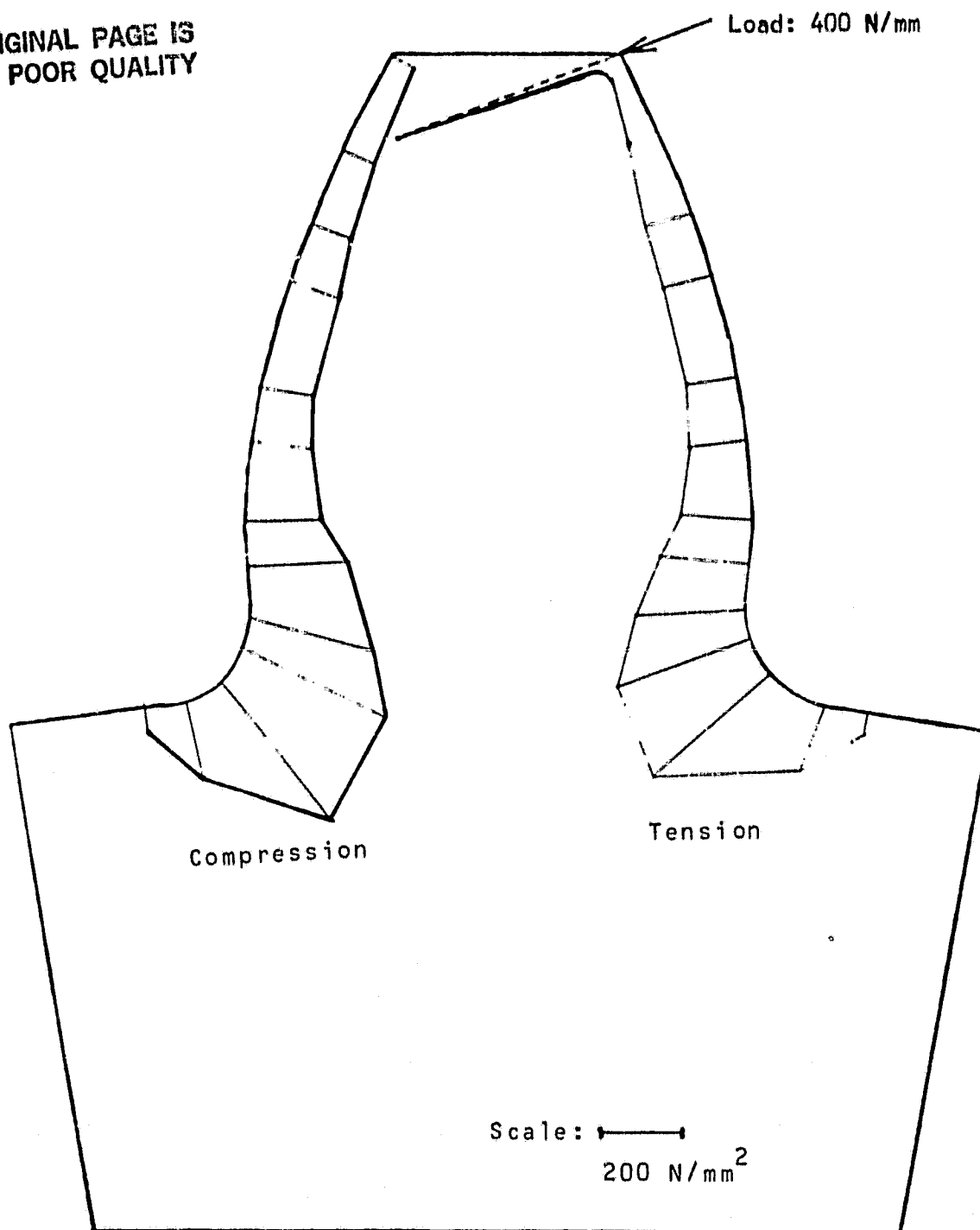


Figure 4. Surface Maximum Stress Distribution for Tip Loading.

ORIGINAL PAGE IS
OF POOR QUALITY

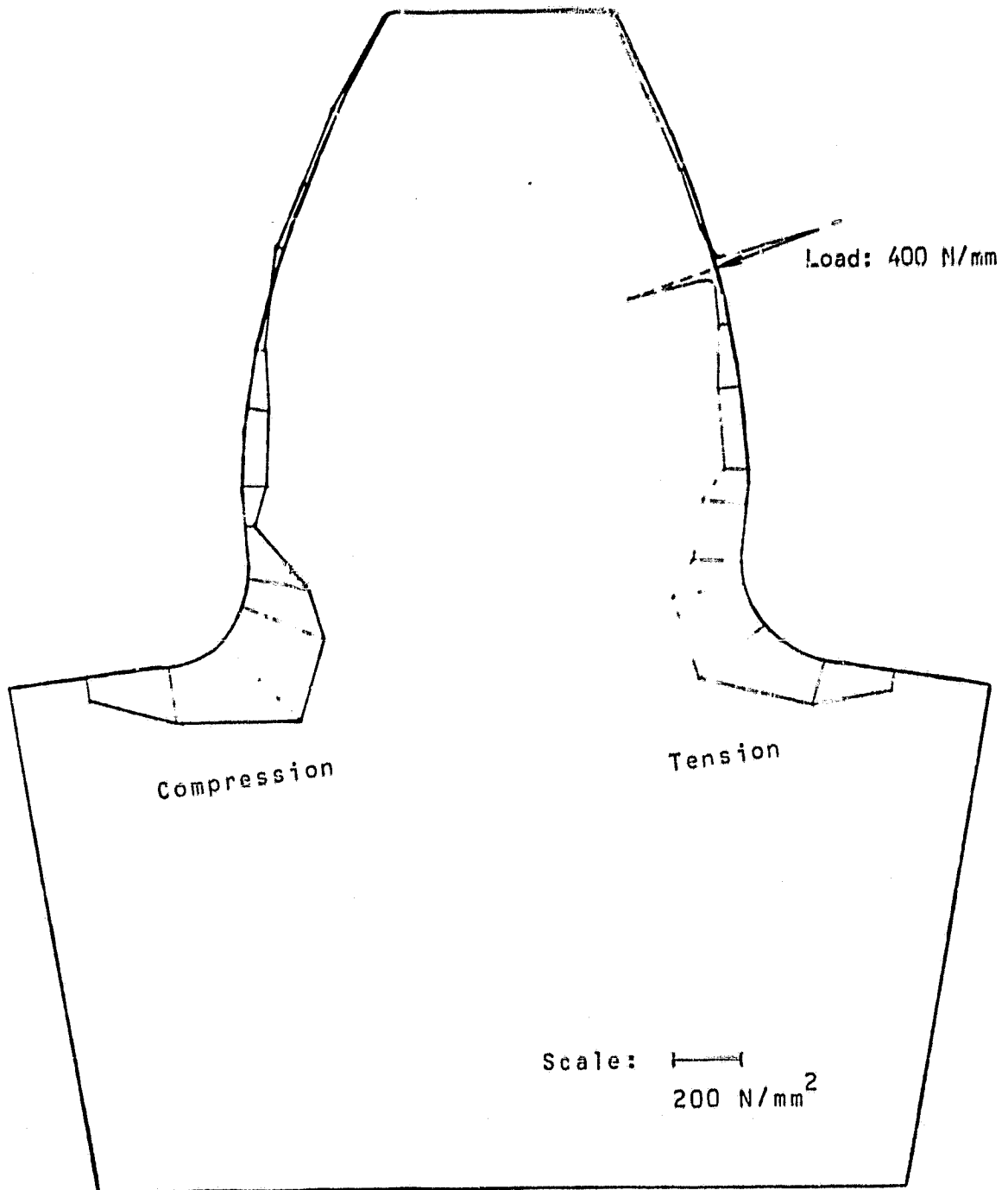


Figure 5. Surface Maximum Stress Distribution for Pitch Point Loading.

ORIGINAL PAGE IS
OF POOR QUALITY

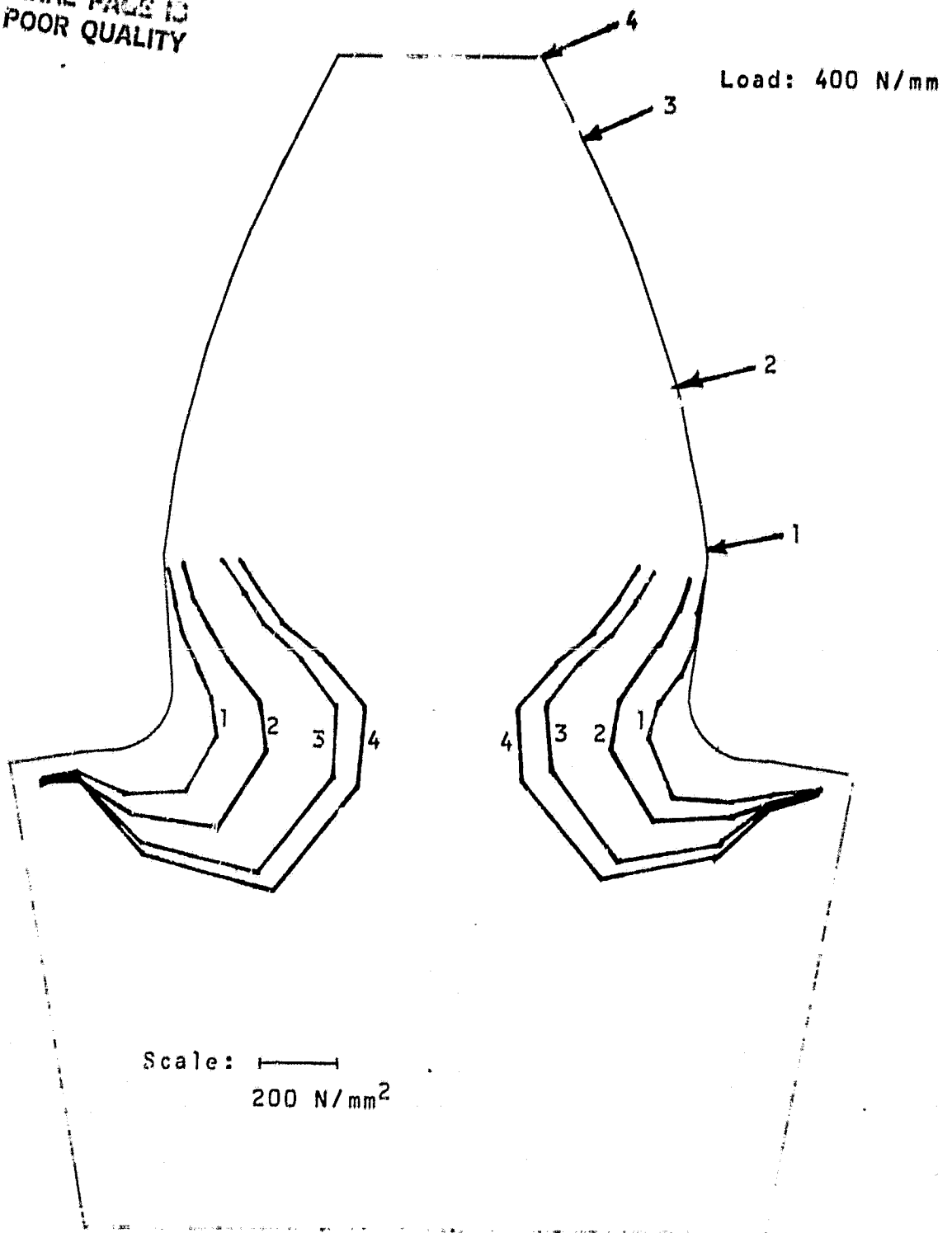


Figure 6. Surface Stress Distribution at the Root for 1.0 mm Root Radius.

ORIGINAL PAGE IS
OF POOR QUALITY

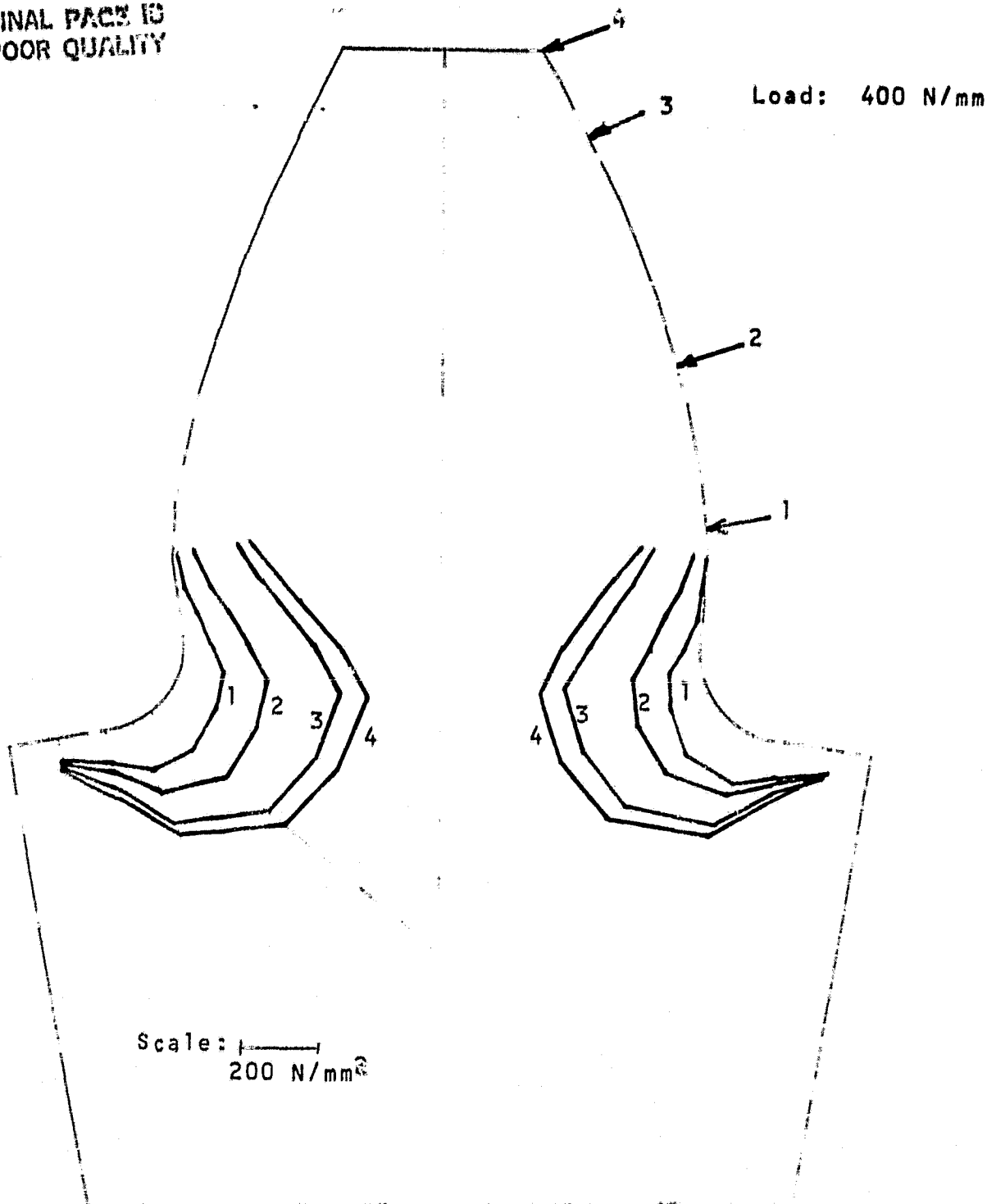


Figure 7. Surface Stress Distribution at the Root for 1.5 mm Root Radius.

ORIGINAL PAGE IS
OF POOR QUALITY

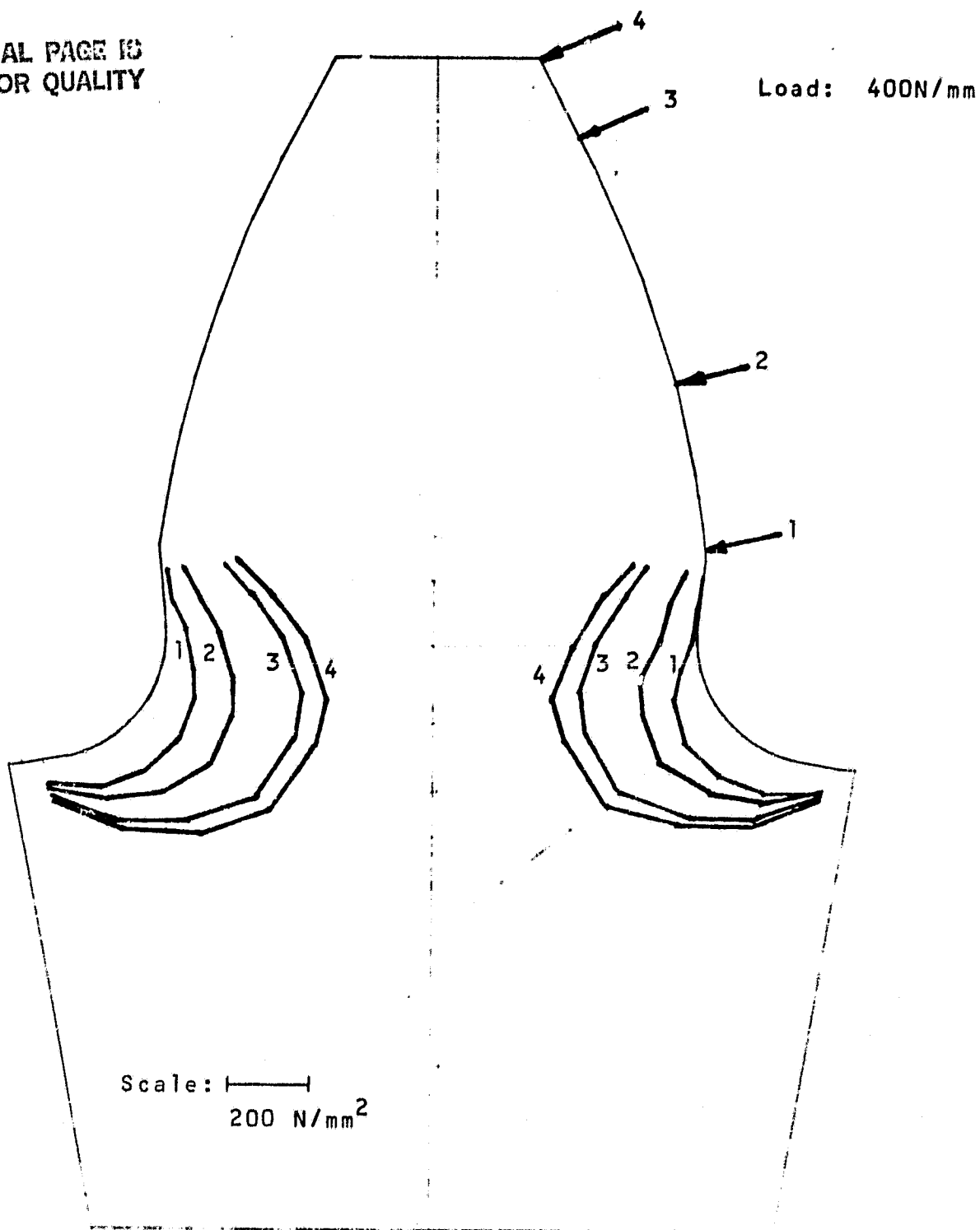


Figure 8. Surface Stress Distribution at the Root for 2.0 mm Root Radius.

Internal Root Section Stresses as a Function of
Root Radius and Loading Position

Figures 9. to 20. show the principal stress distribution across the root section for the loading points of Figure 3. for the various root radii. As expected, the stresses are smallest at the center of the section and the largest stresses occur at the root surface. Interestingly, the root radius has little effect upon the internal stress distribution.

Effect of Rim Thickness and Support Conditions

Figures 21. to 41. show the effect of the rim thickness and the hub or rim support upon the root stresses and the stresses across the root section. Specifically, Figures 21. and 22. show the root surface stresses for a gear tooth with a fully supported rim (that is, supported at the rim base and along the radial sides, simulating tight fitting hubs). The root radius was 2.0 mm and the rim radii were 35.0 mm and 37.1 mm. The loading was the same as that shown in Figure 3.

Similarly, Figures 23. and 24. show the root surface stresses for a gear tooth with a partially supported rim (that is, supported only along the radial sides, simulating loose fitting hubs). The root radii, rim radii and loading were the same as with the fully supported rim.

These results show that when the rim is fully supported the root surface stresses decrease slightly as the rim thickness decreases. However, when the rim is only partially supported the root surface stresses increase substantially as

ORIGINAL PAGE IS
OF POOR QUALITY

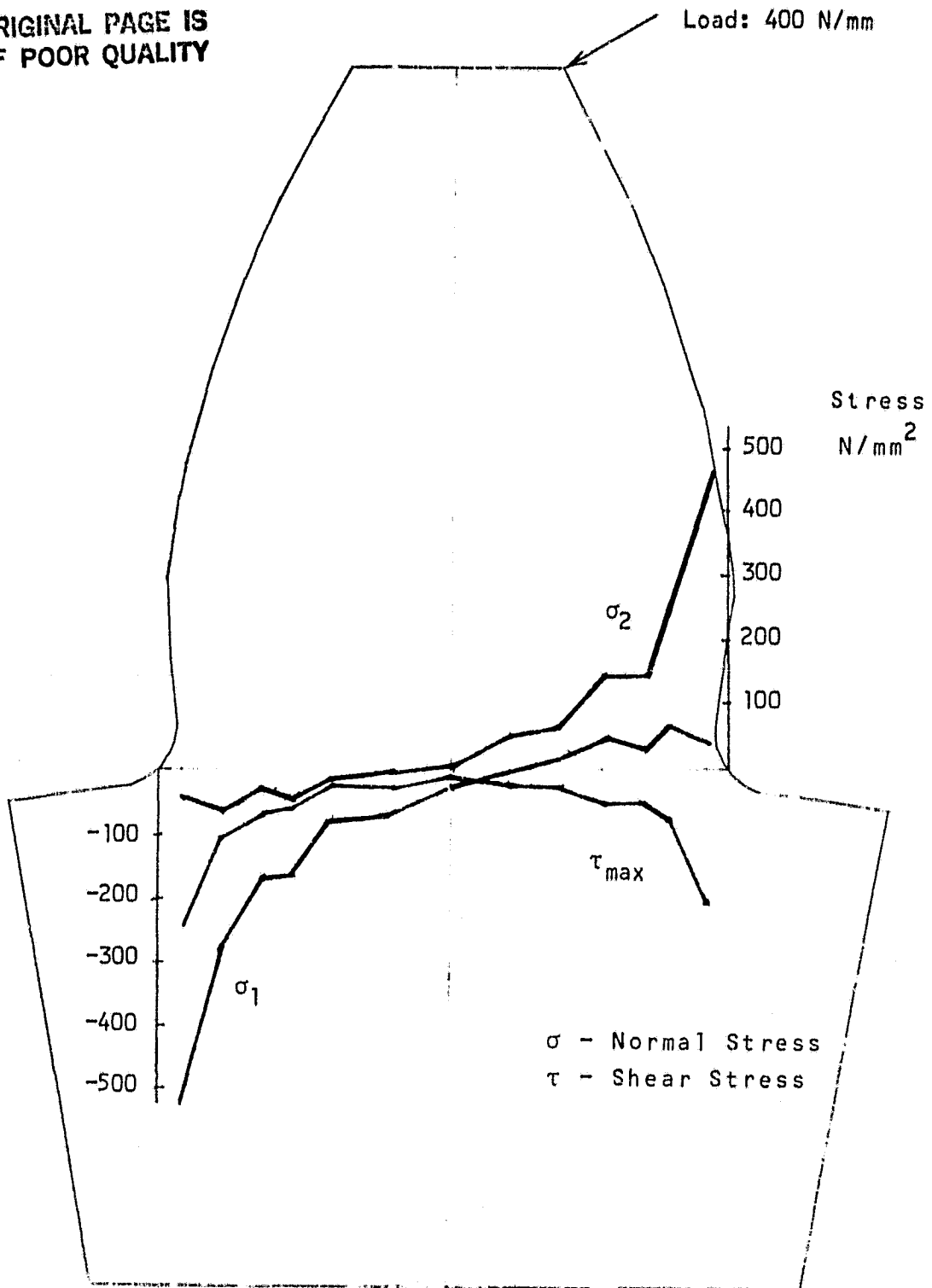


Figure 9. Internal Root Section Principal Stresses
for Tip Loading for 1.0 mm Root Radius.

ORIGINAL PAGE IS
OF POOR QUALITY

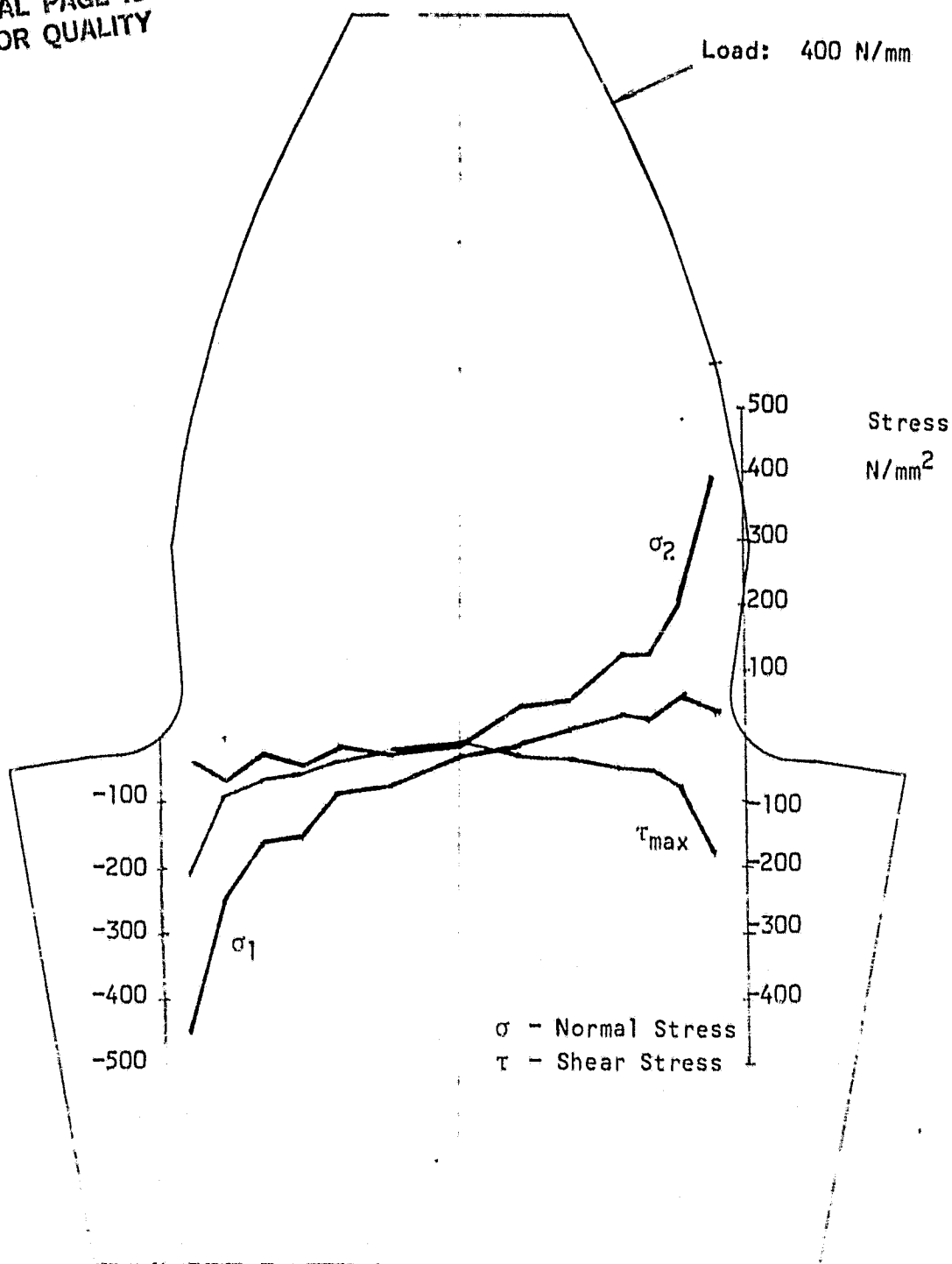


Figure 10. Internal Root Section Principal Stresses for Near-Tip Loading for 1.0 mm Root Radius.

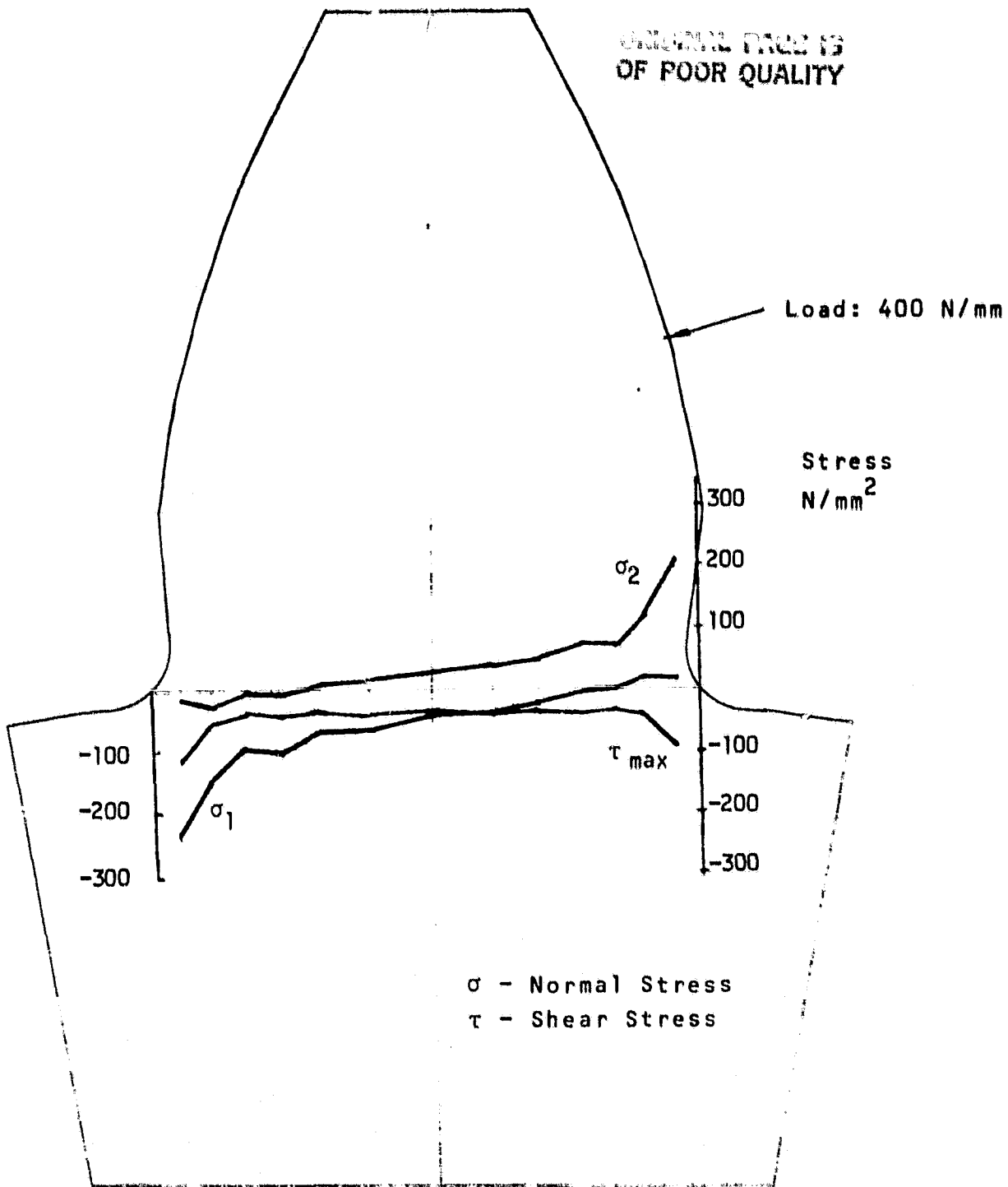


Figure 11. Internal Root Section Principal Stresses for Pitch Point Loading for 1.0 mm Root Radius.

ORIGINAL PAGE IS
OF POOR QUALITY

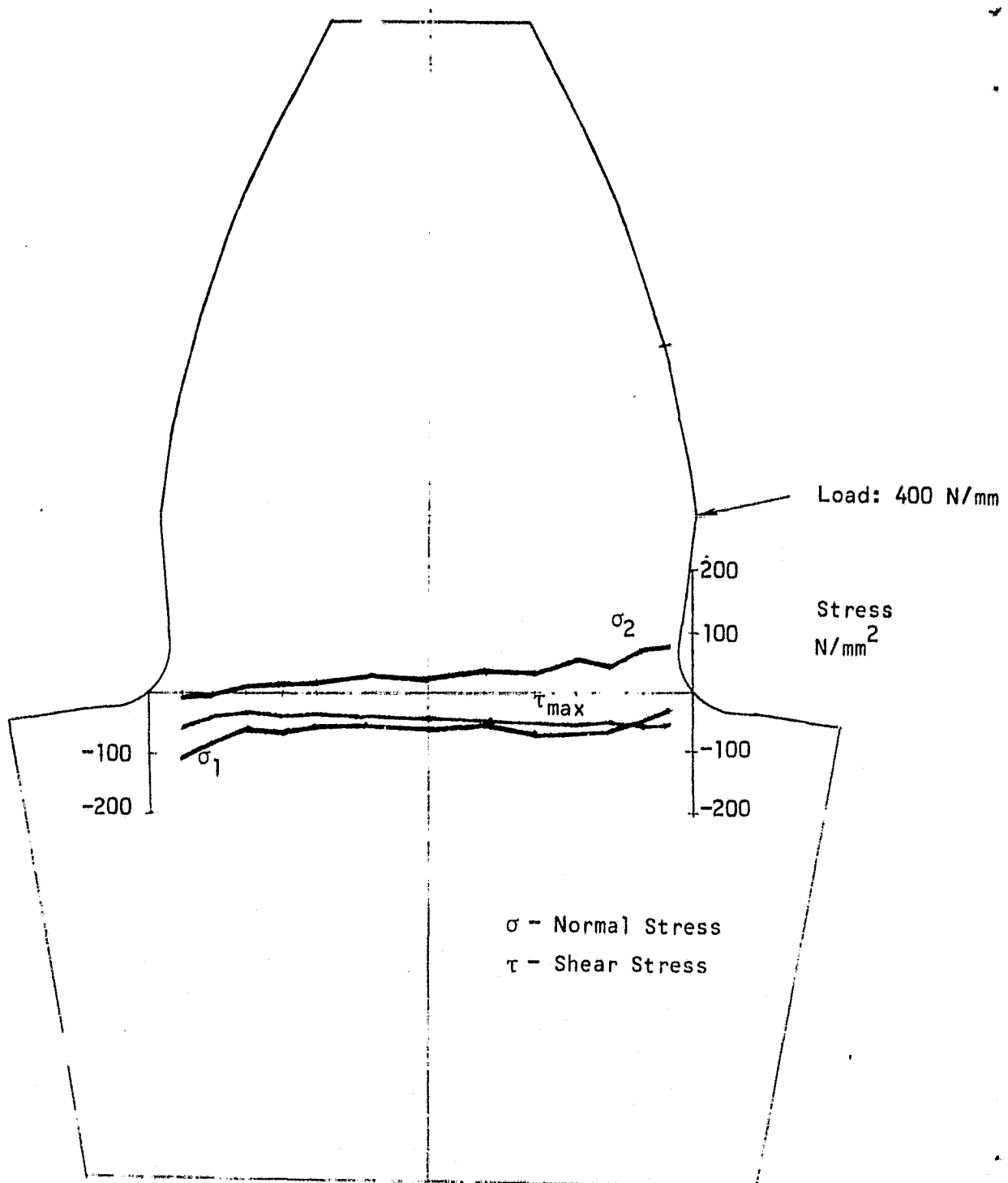


Figure 12. Internal Root Section Principal Stresses
for Near-Root Loading for 1.0 mm Root Radius.

ORIGINAL DRAFT
OF POOR QUALITY

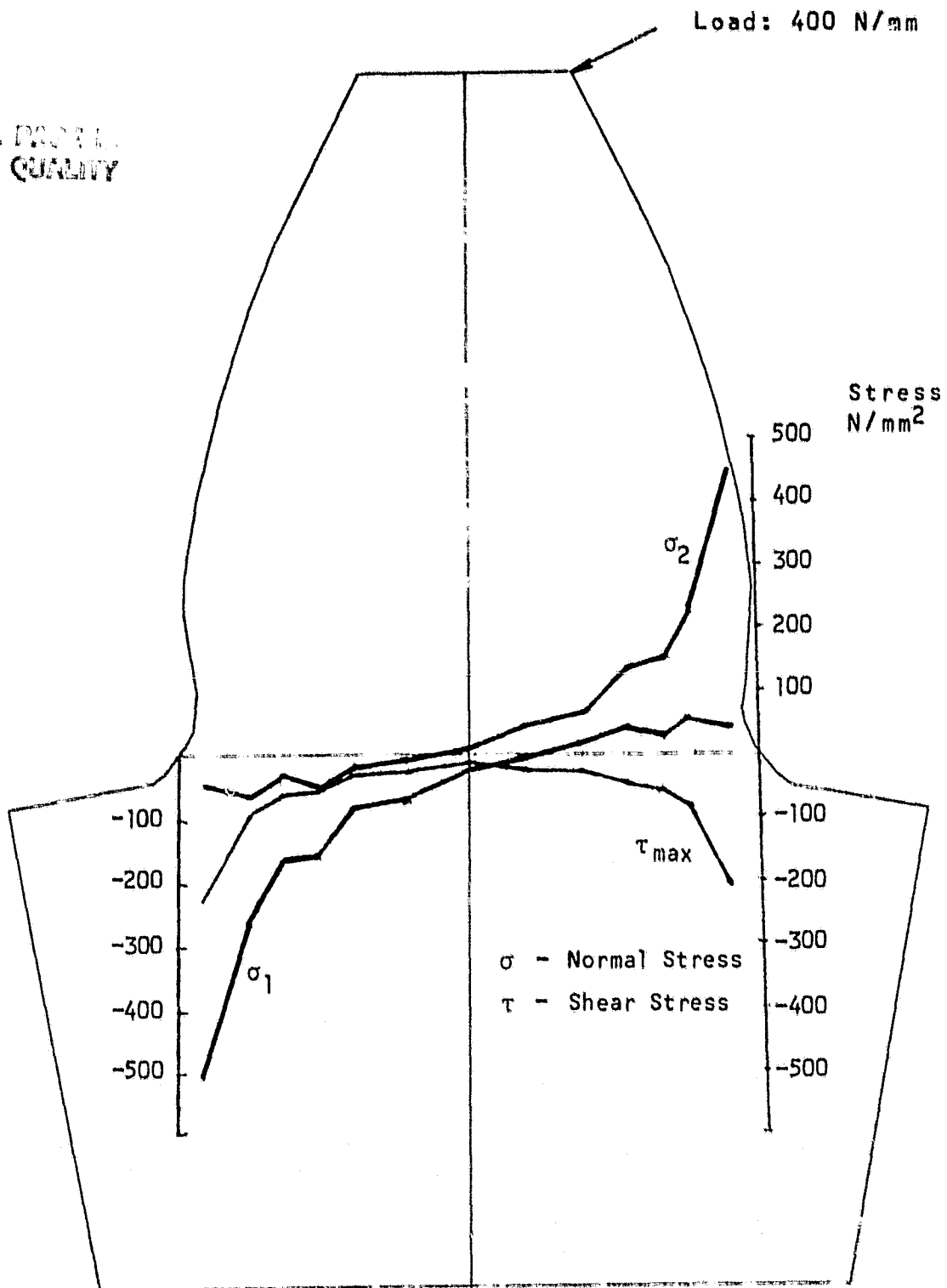


Figure 13. Internal Root Section Principal Stresses for Tip Loading for 1.5 mm Root Radius.

ORIGINAL PAGE IS
OF POOR QUALITY

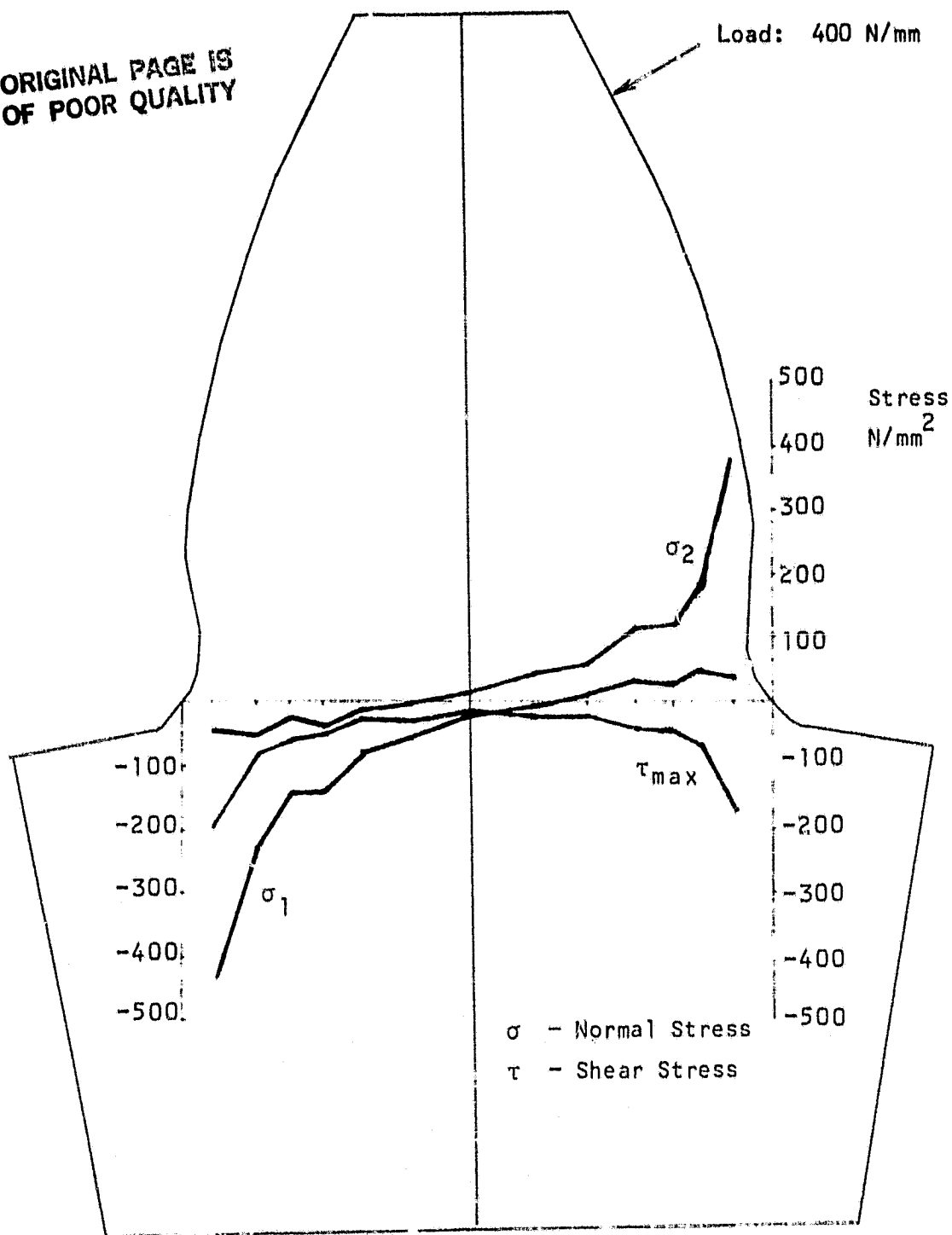


Figure 14. Internal Root Section Principal Stresses for Near-Tip Loading for 1.5 mm Root Radius.

ORIGINAL PARTIAL
OF POOR QUALITY

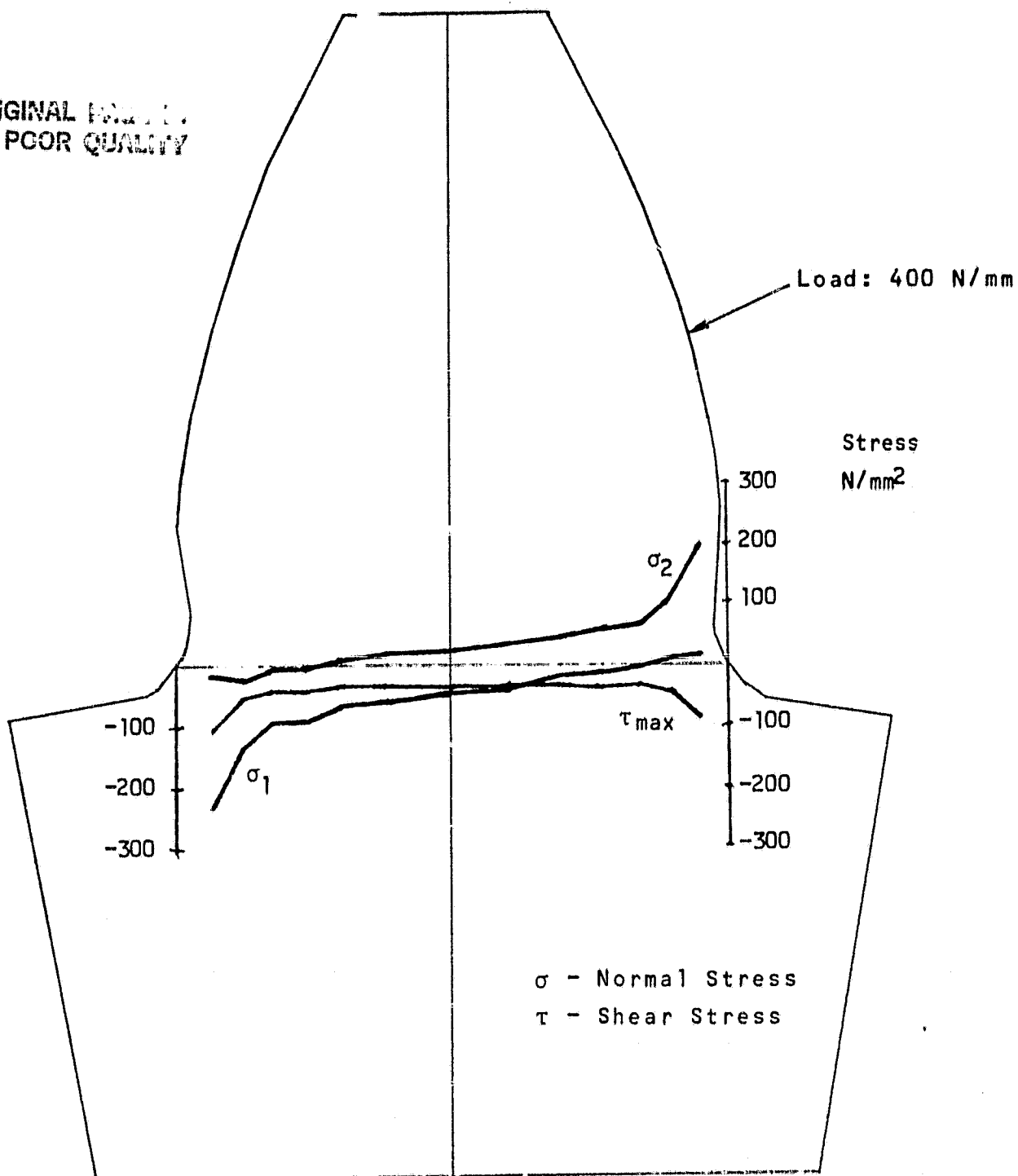


Figure 15. Internal Root Section Root Section Principal Stresses for Pitch Point Loading for 1.5 mm Root Radius.

ORIGINAL PAGE IS
OF POOR QUALITY

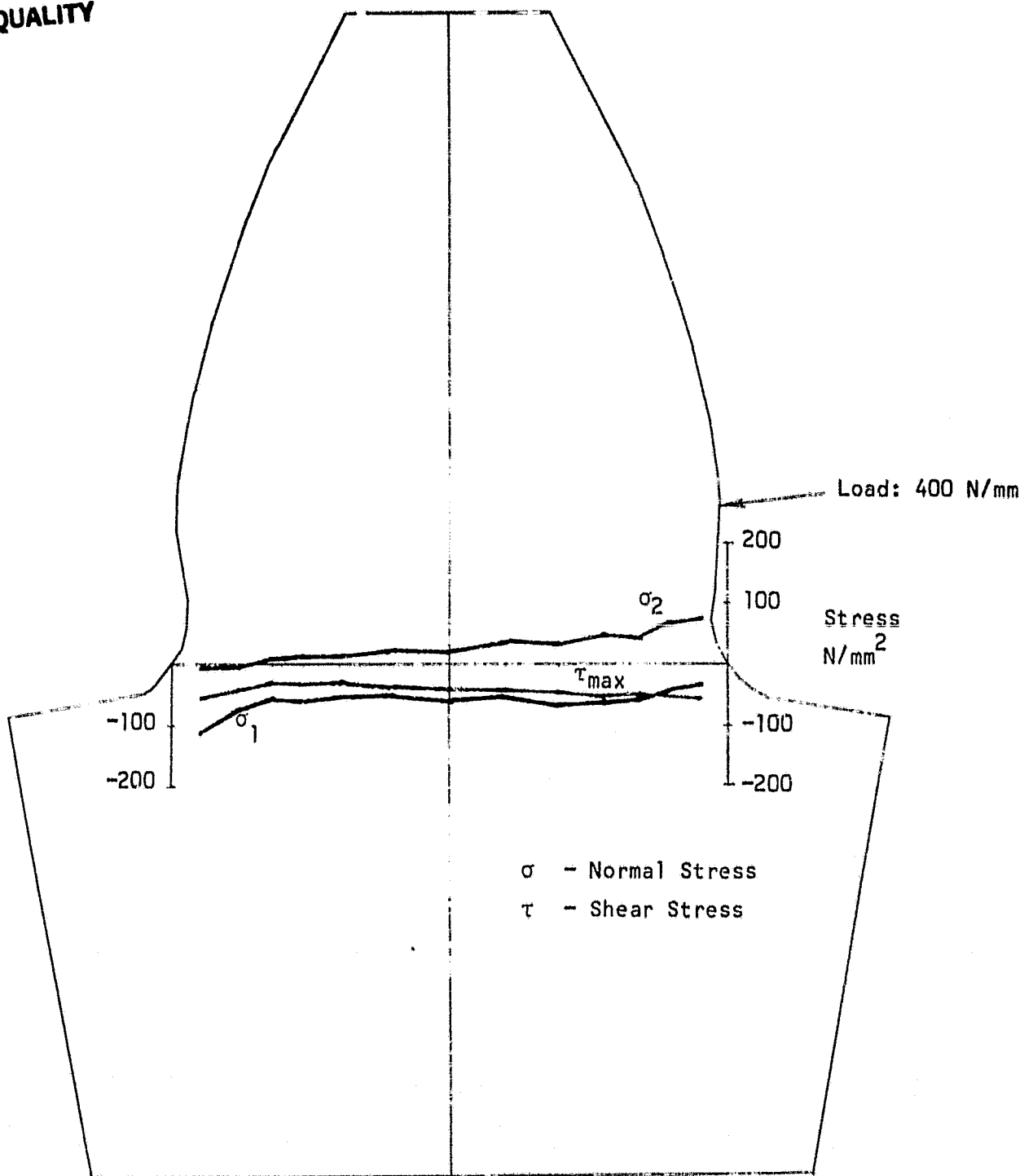


Figure 16. Internal Root Section Principal Stresses for Near-Root Loading for 1.5 mm Root Radius.

ORIGINAL POINTS
OF POOR QUALITY

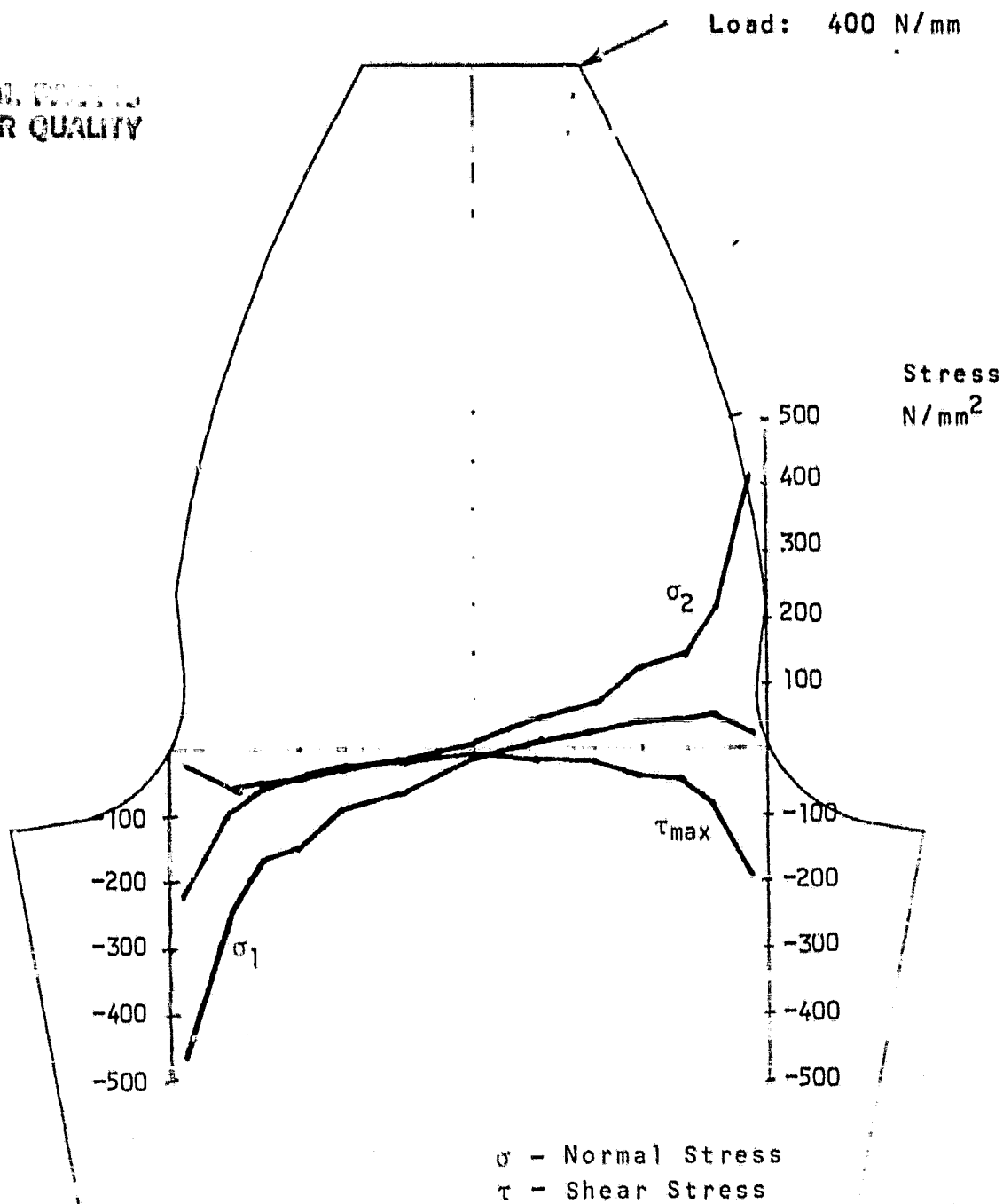


Figure 17. Internal Root Section Principal Stresses for Tip Loading for 2.0 mm Root Radius.

ORIGINAL PAGE IS
OF POOR QUALITY

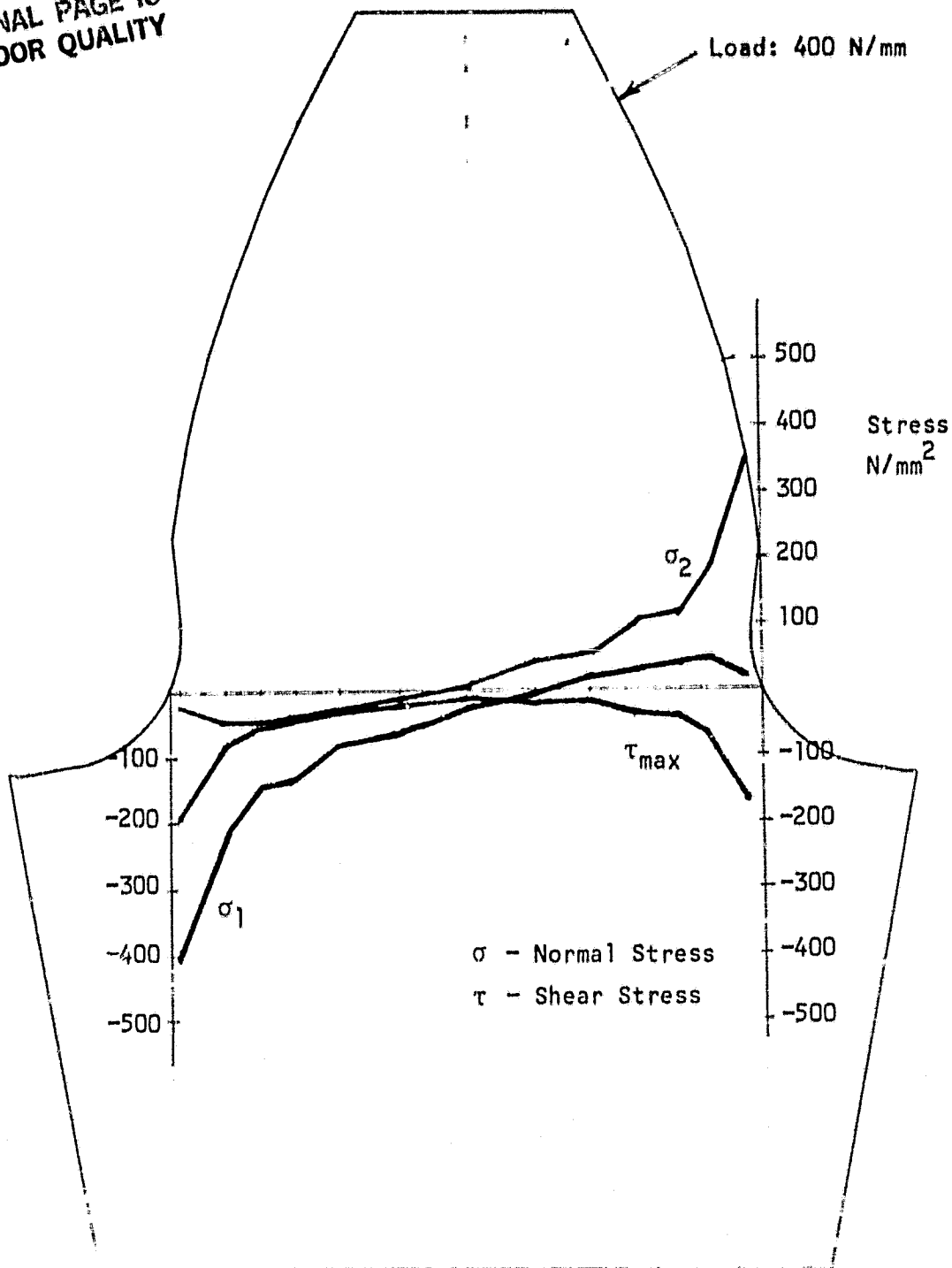


Figure 18. Internal Root Section Principal Stresses
for Near-Tip Loading for 2.0 mm Root Radius.

ORIGINAL PAGE IS
OF POOR QUALITY

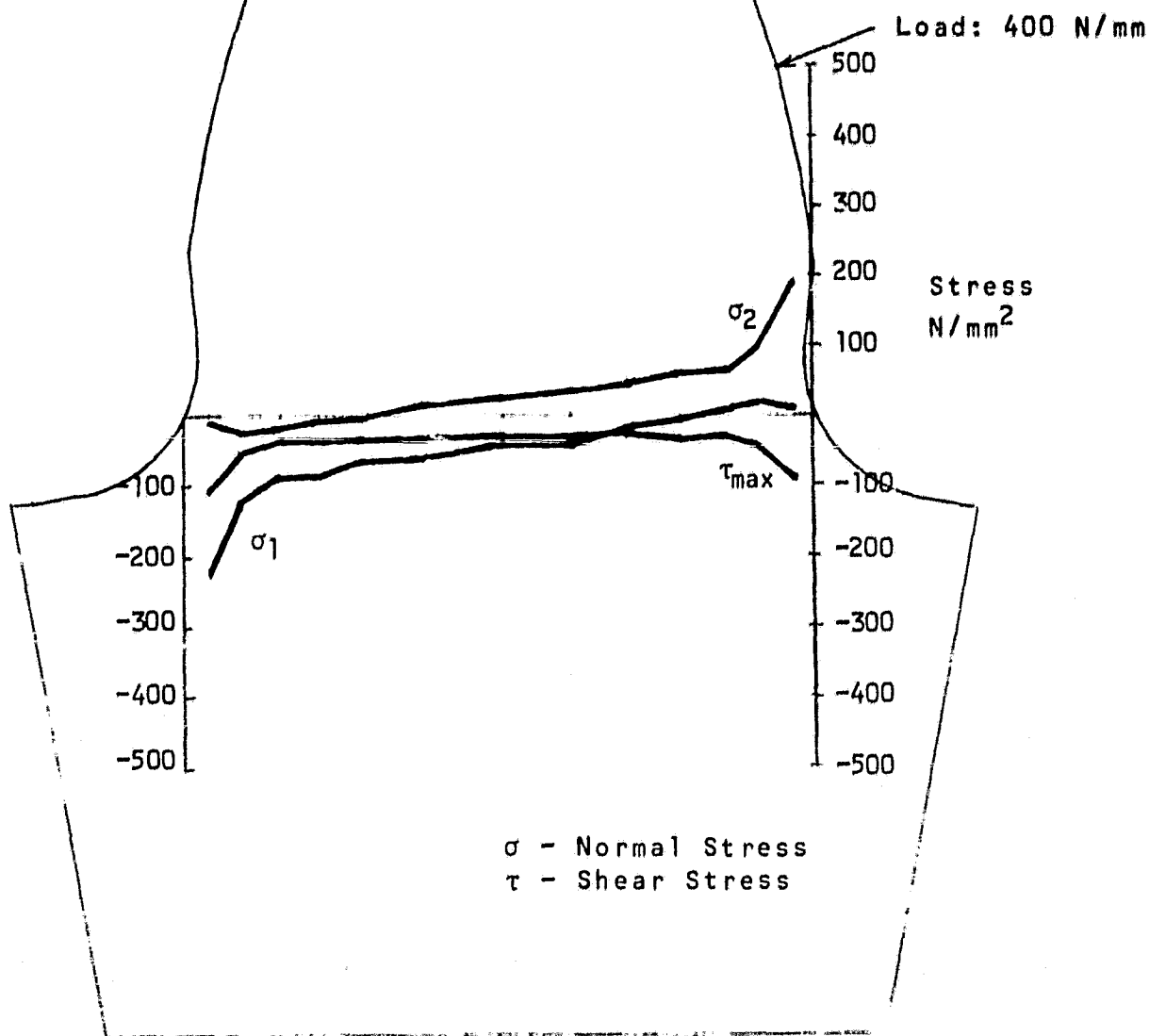


Figure 19. Internal Root Section Principal Stresses for Pitch Point Loading for 2.0 mm Root Radius.

ORIGINAL PAGE IS
OF POOR QUALITY

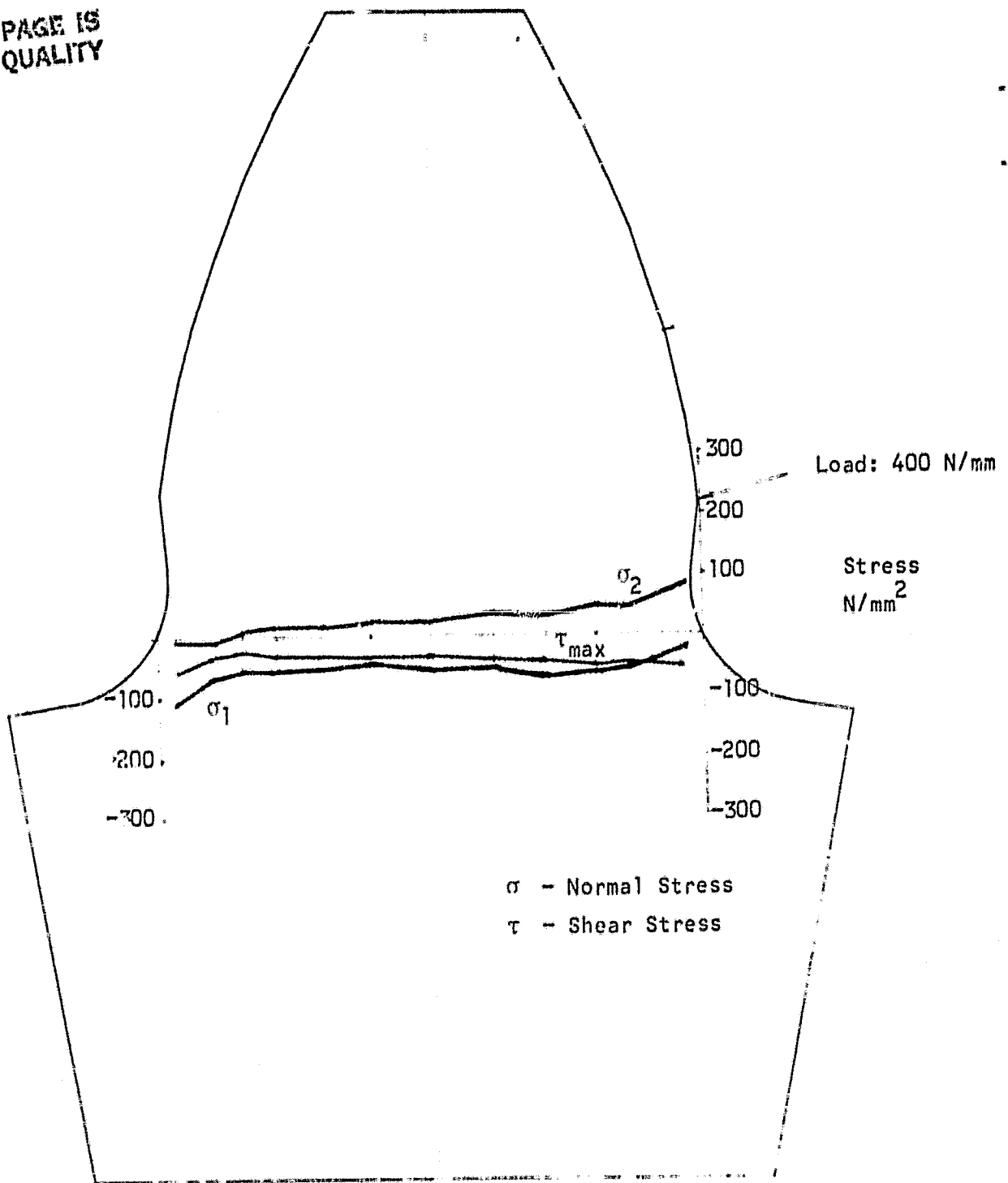


Figure 20. Internal Root Section Principal Stresses for Near-Root Loading for 2.0 mm Root Radius.

ORIGINAL PAGE IS
OF POOR QUALITY

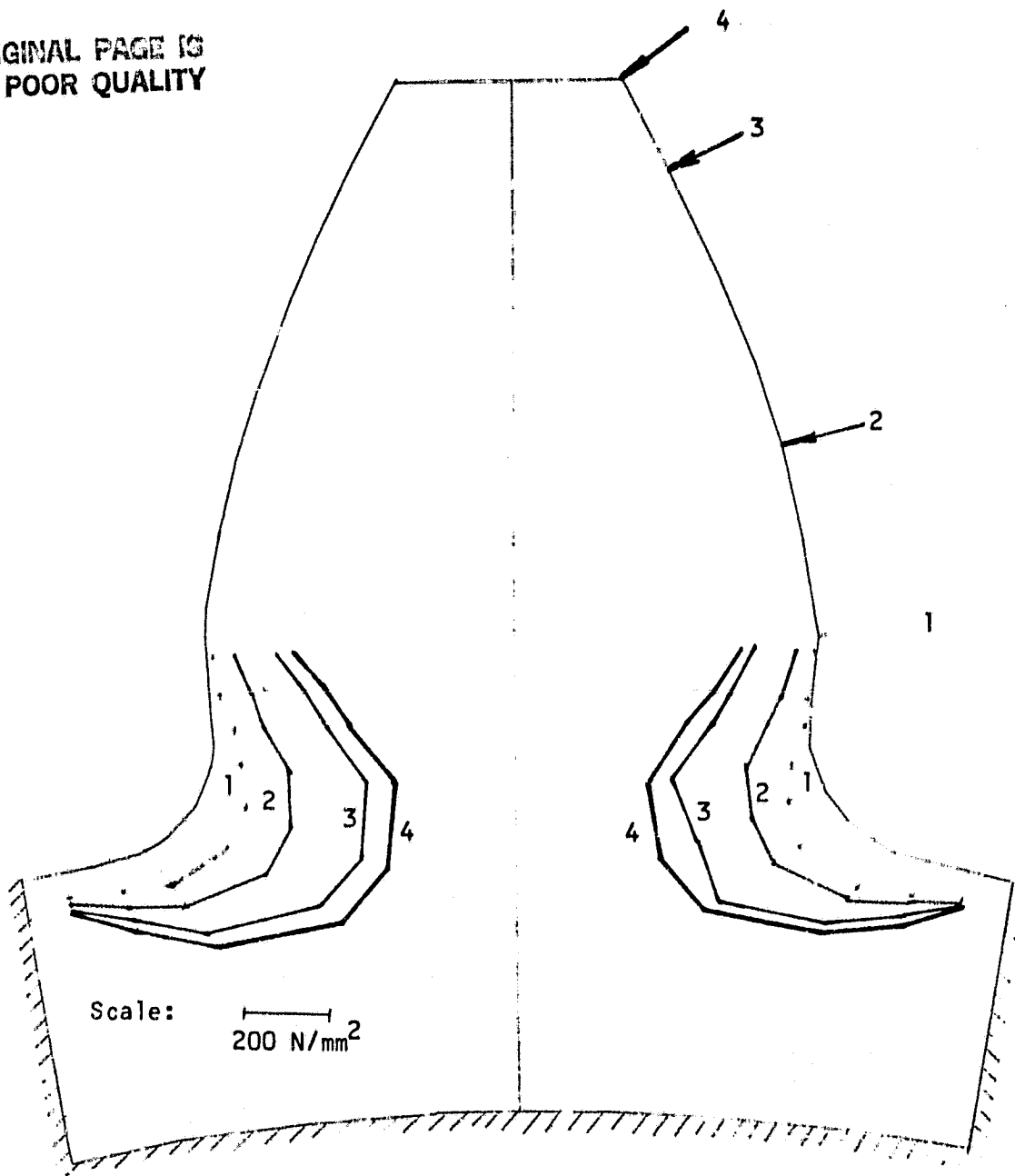
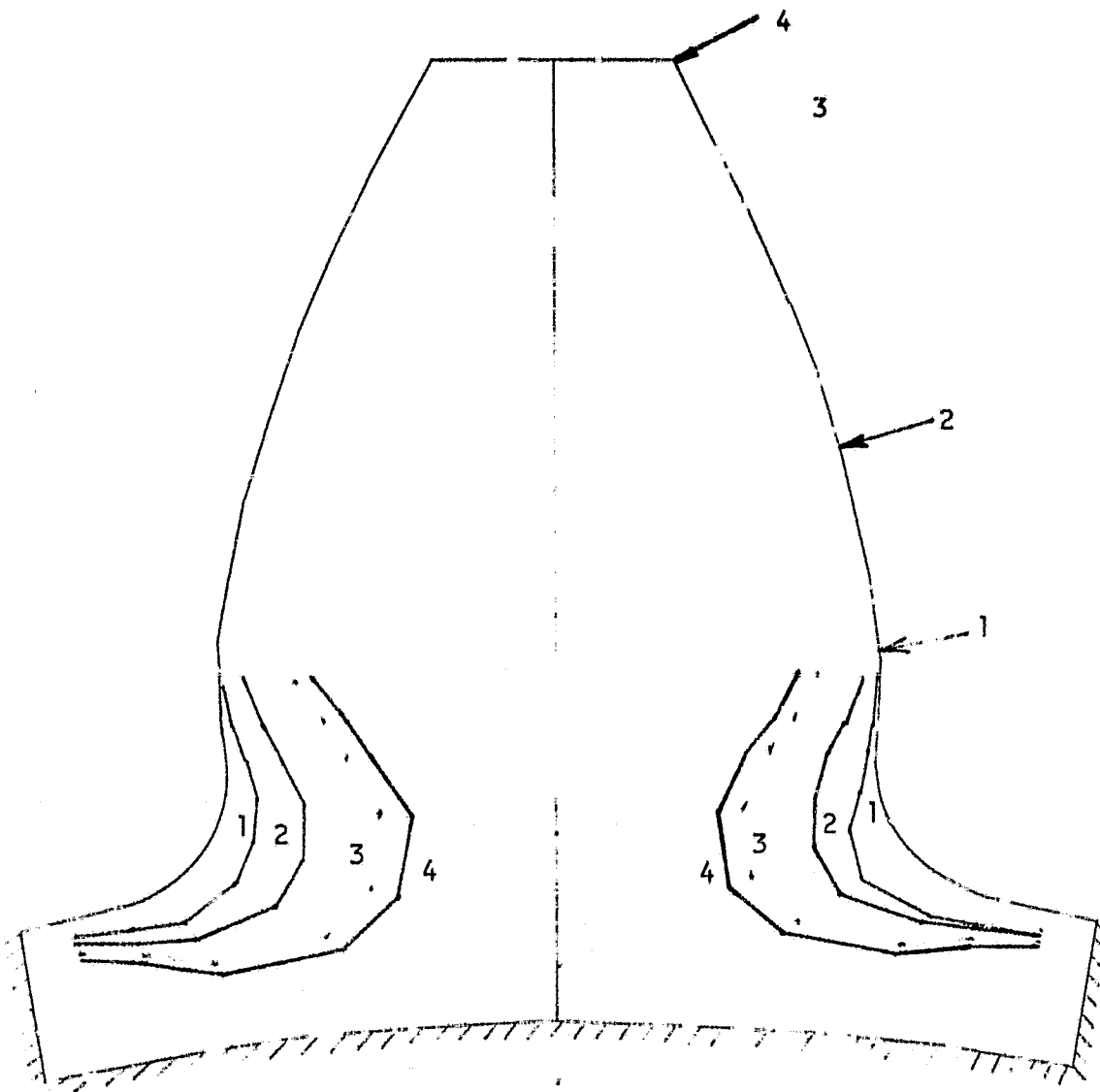


Figure 21. Surface Stress Distribution at the Root for a Fully Supported Rim with a Rim Radius of 35 mm.

ORIGINAL PAGE IS
OF POOR QUALITY



Scale: 200 N/mm^2

Figure 22. Surface Stress Distribution at the Root for a Fully Supported Rim with a Rim Radius of 37.1 mm.

ORIGINAL PAGE IS
OF POOR QUALITY

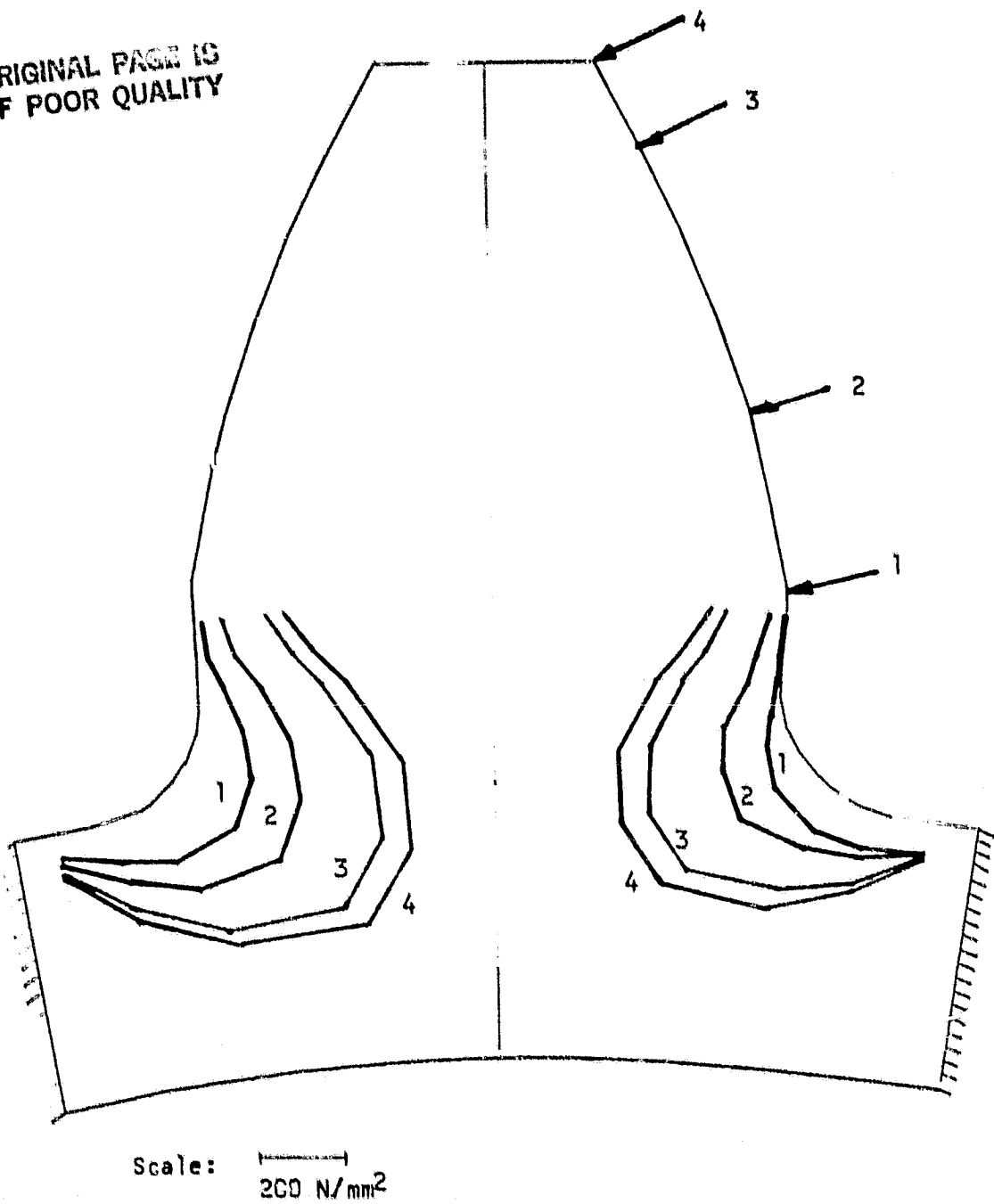


Figure 23. Surface Stress Distribution at the Root for a Partially Supported Rim with a Rim Radius of 35 mm.

ORIGINAL PAGE IS
OF POOR QUALITY

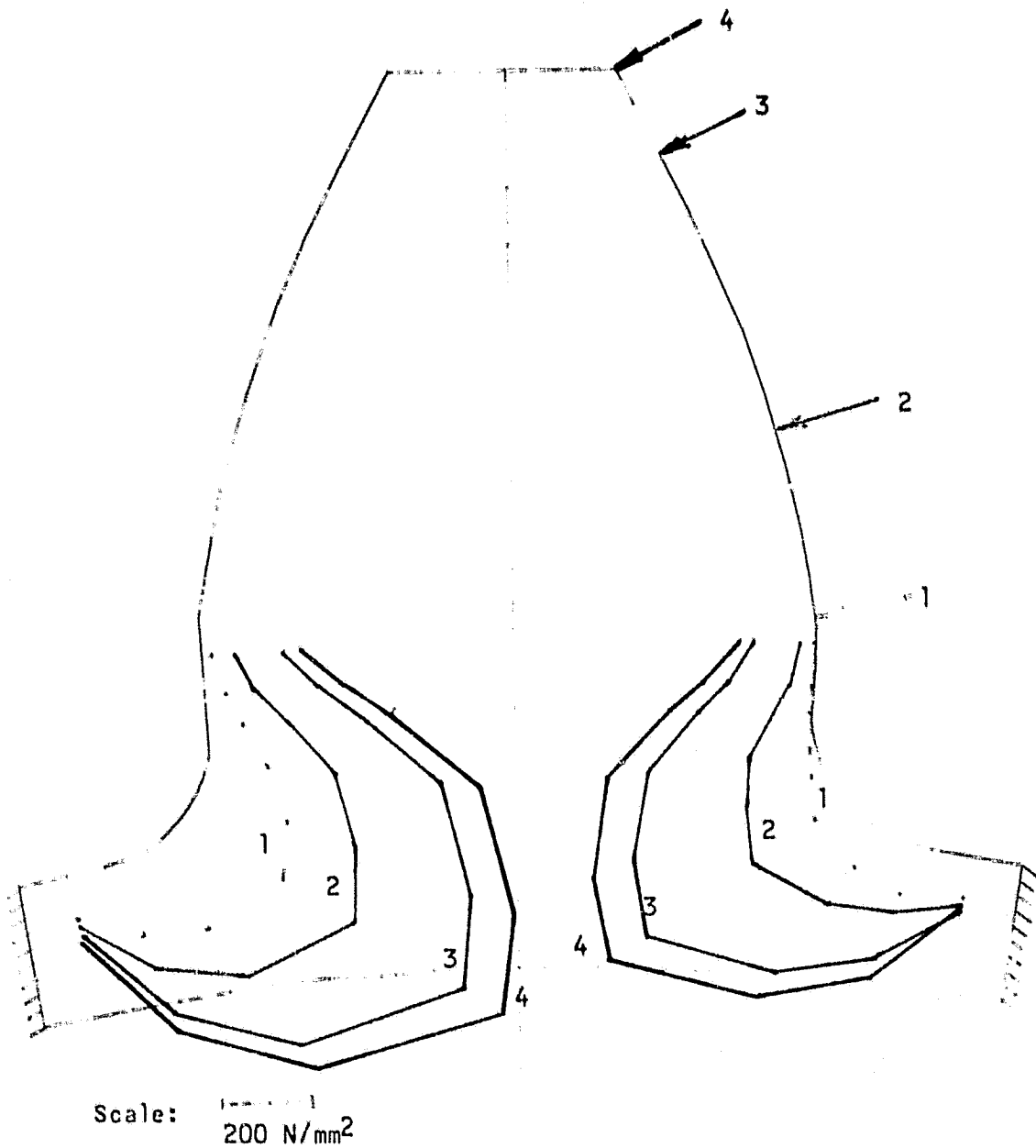


Figure 24. Surface Stress Distribution at the Root for a Partially Supported Rim with a Rim Radius of 37.1 mm.

ORIGINAL PAGE IS
OF POOR QUALITY

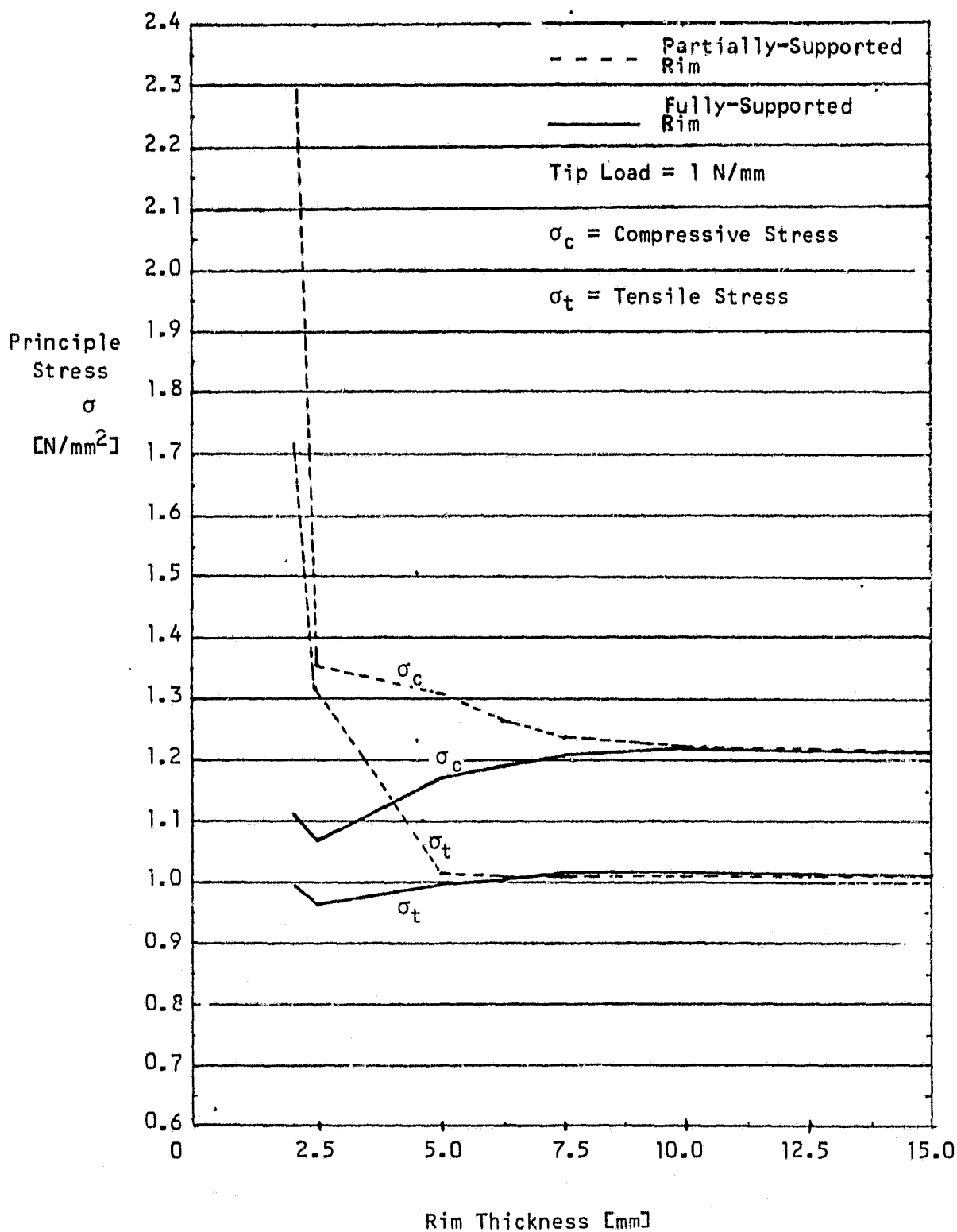


Figure 25. Variation of Maximum Root Stresses with Rim Thickness.

ORIGINAL PAGE IS
OF POOR QUALITY

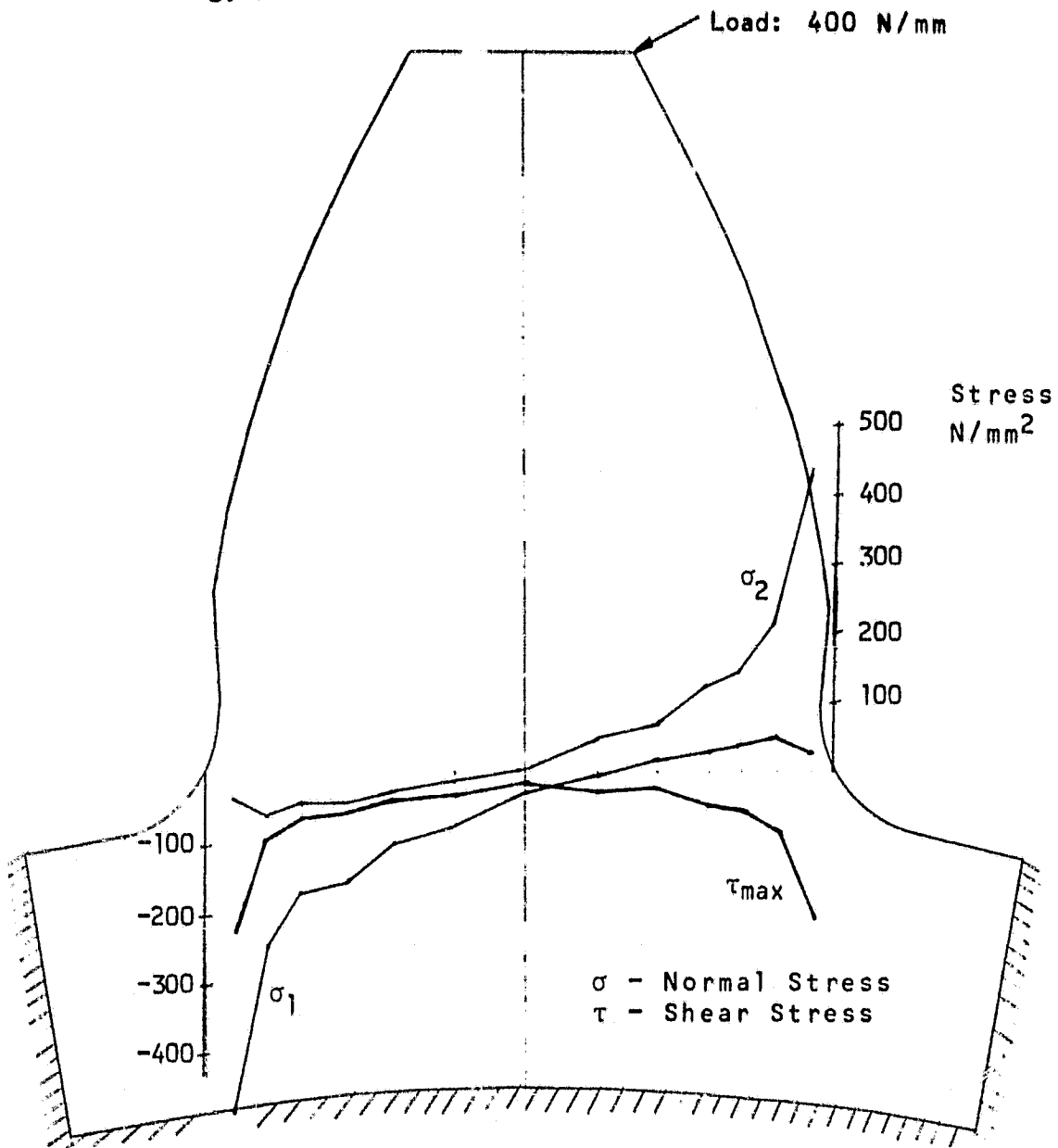


Figure 26. Internal Root Section Principal Stresses for a Fully Supported Rim with Tip Loading with a Rim Radius of 35 mm.

ORIGINAL PAGE IS
OF POOR QUALITY

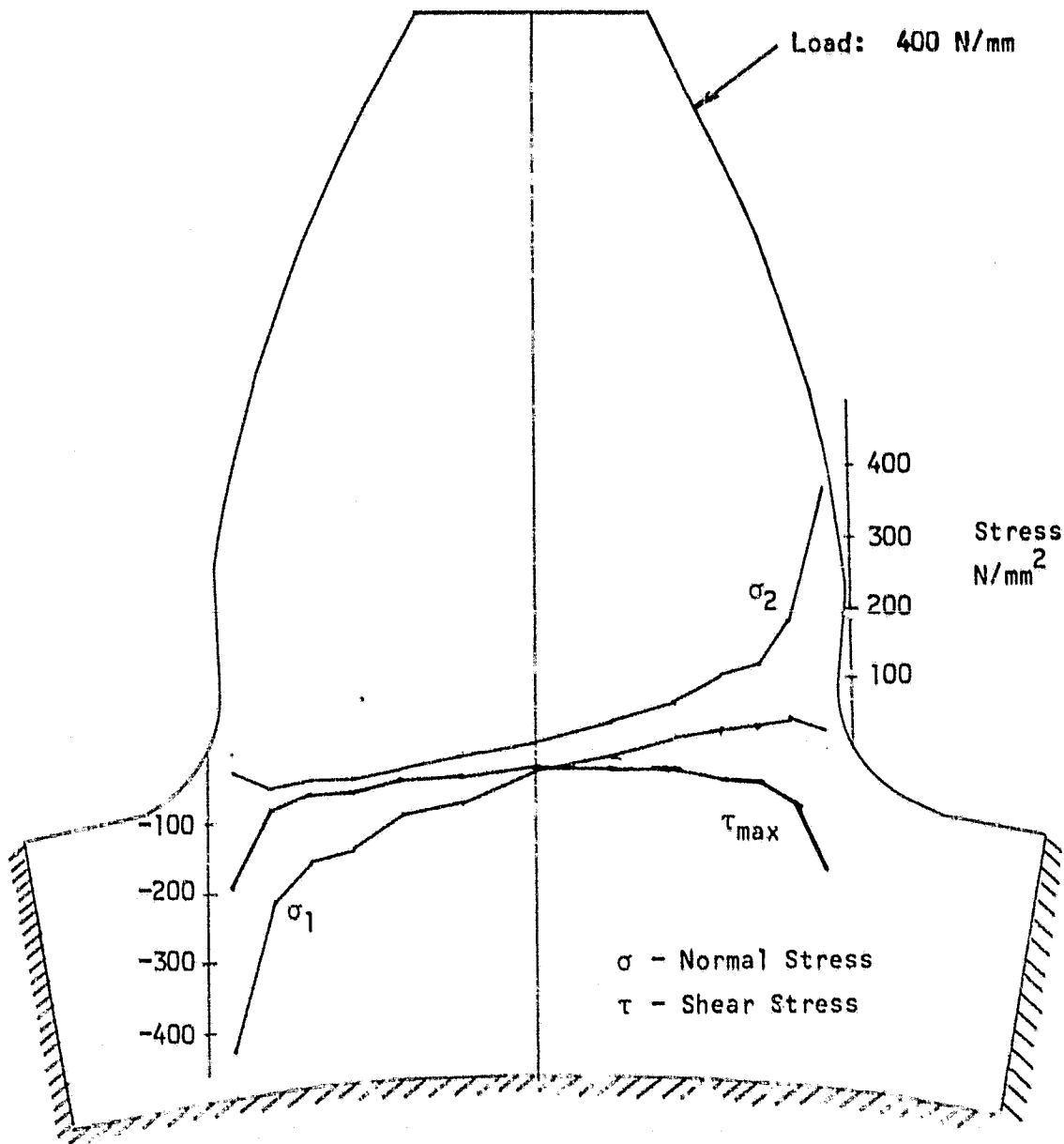


Figure 27. Internal Root Section Principal Stresses for a Fully Supported Rim with Near-Tip Loading with a Rim Radius of 35 mm.

ORIGINAL PAGE IS
OF POOR QUALITY

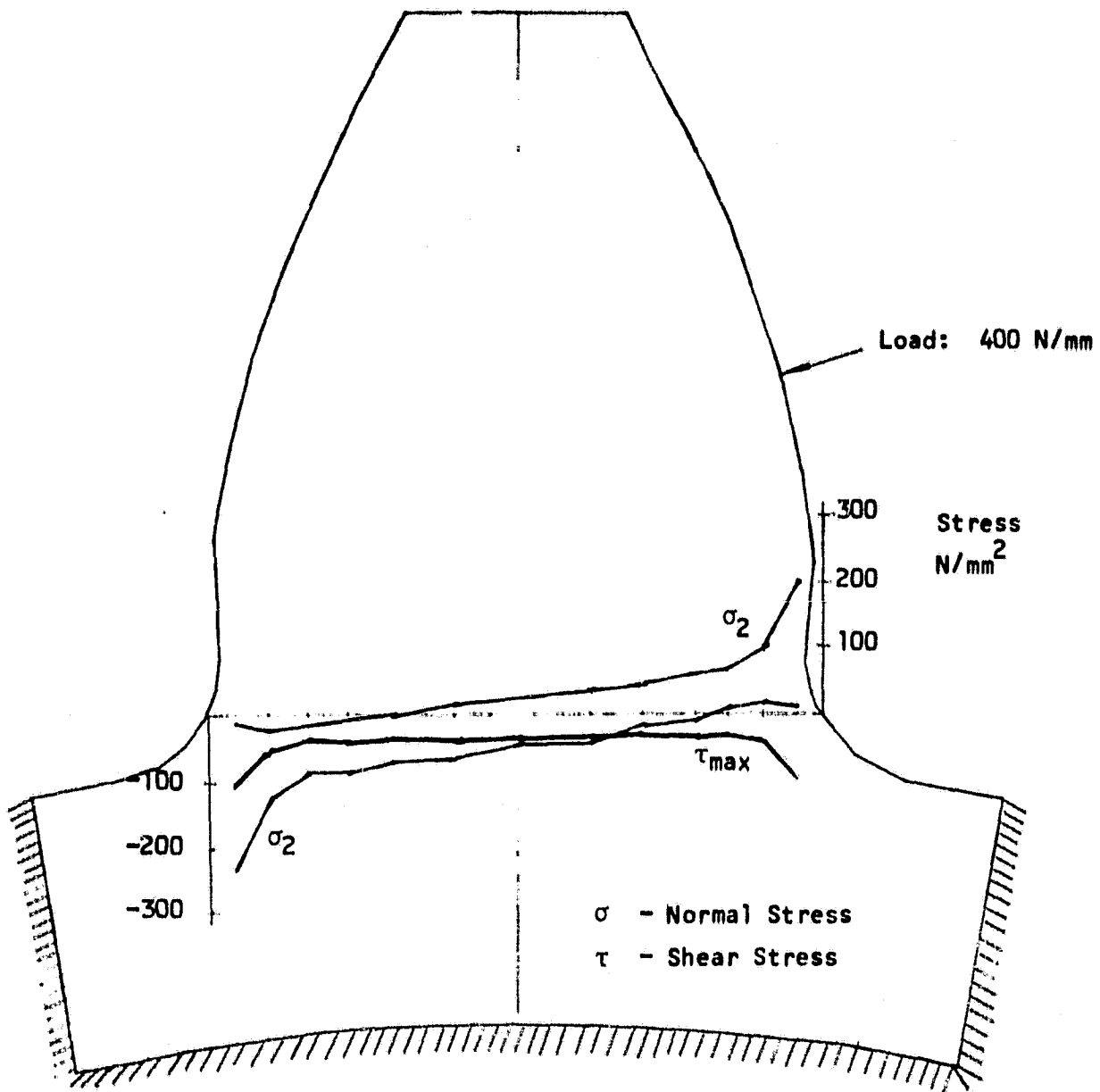


Figure 28. Internal Root Section Principal Stresses for a Fully Supported Rim with Pitch Point Loading with a Rim Radius of 35 mm.

ORIGINAL PAGE 13
OF POOR QUALITY

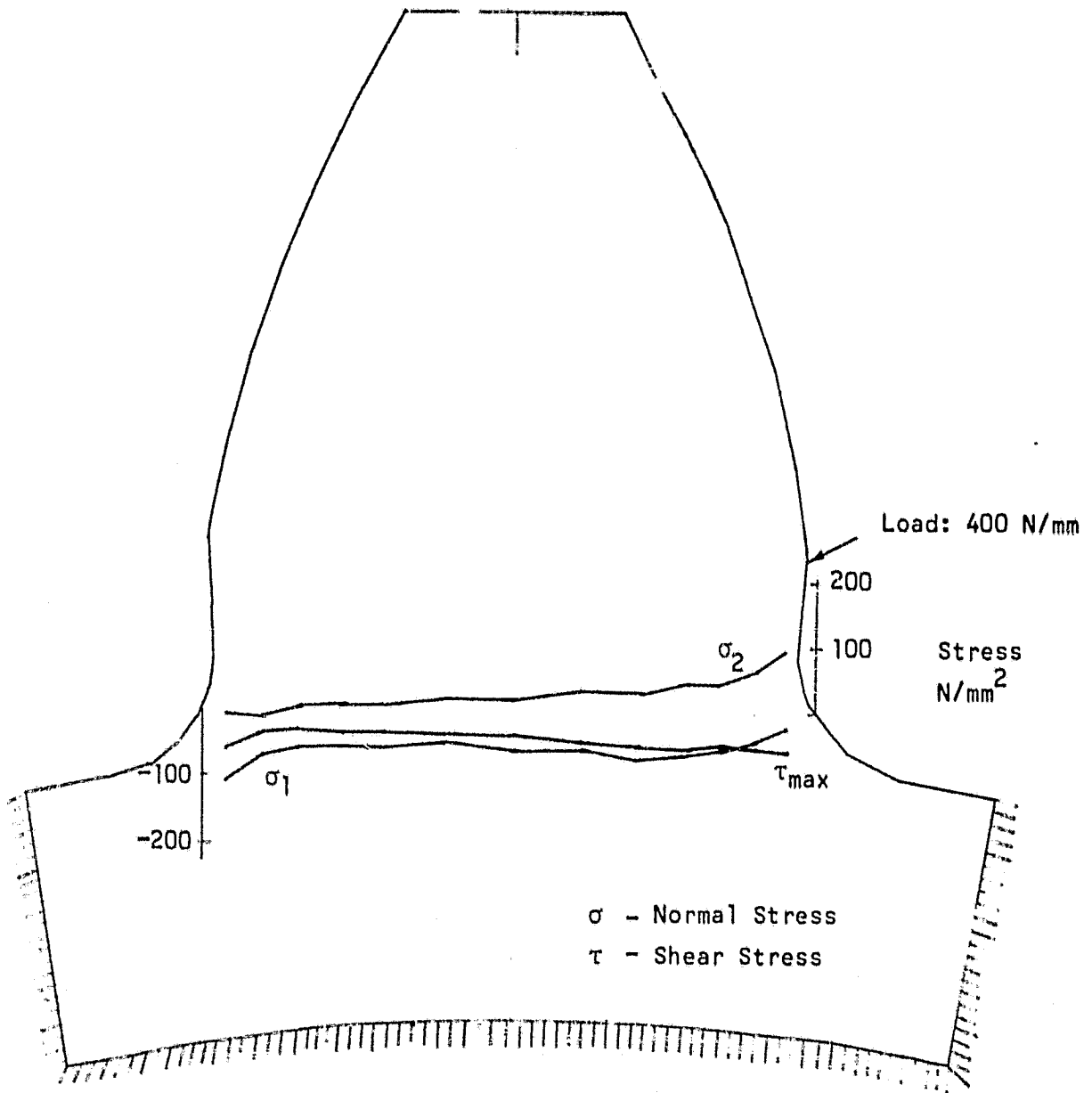


Figure 29. Internal Root Section Principal Stresses for a Fully Supported Rim with Near-Root Loading with a Rim Radius of 35 mm.

ORIGINAL PAGE IS
OF POOR QUALITY

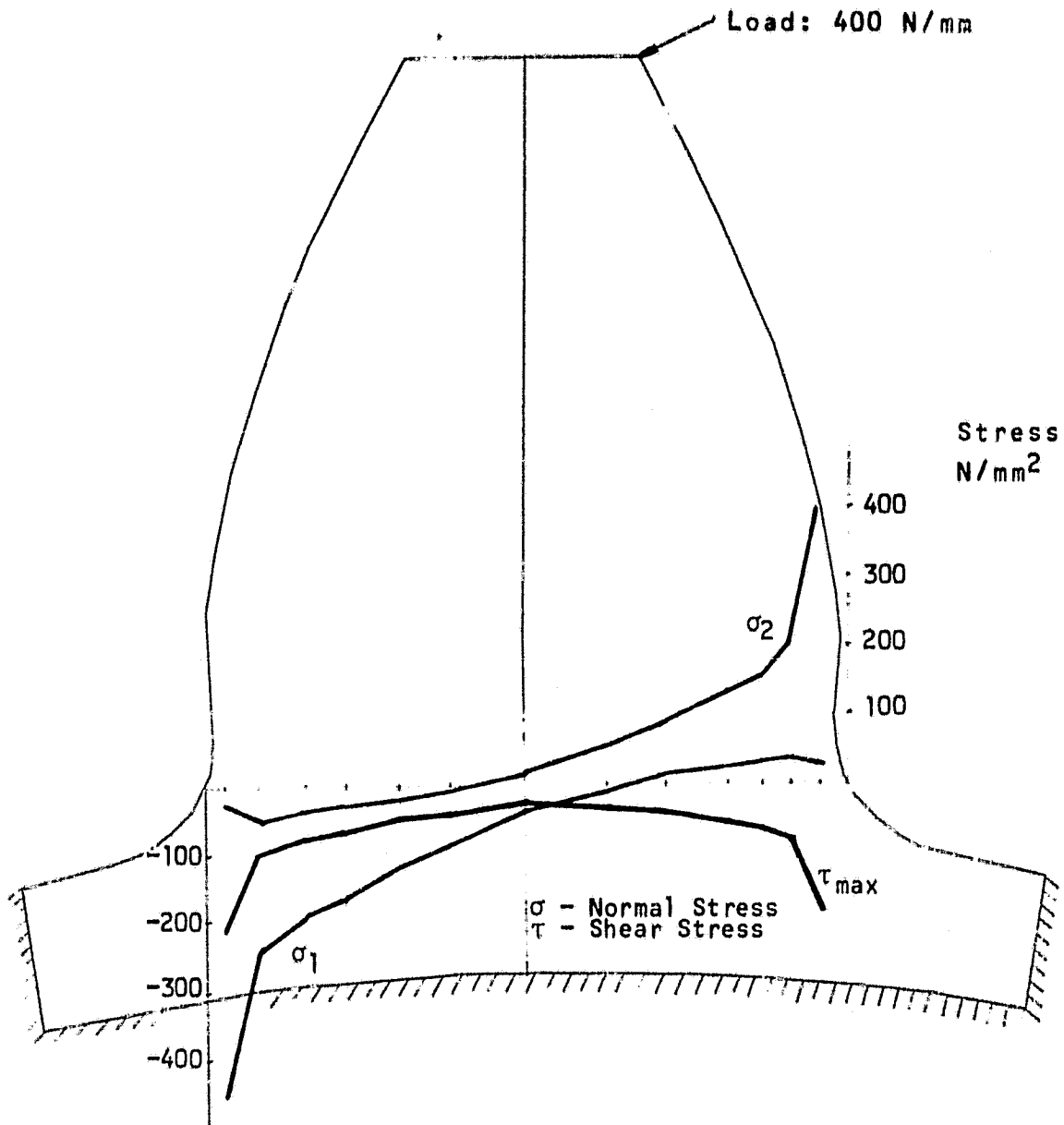


Figure 30. Internal Root Section Principal Stresses for a Fully Supported Rim with Tip Loading with a Rim Radius of 37.1 mm.

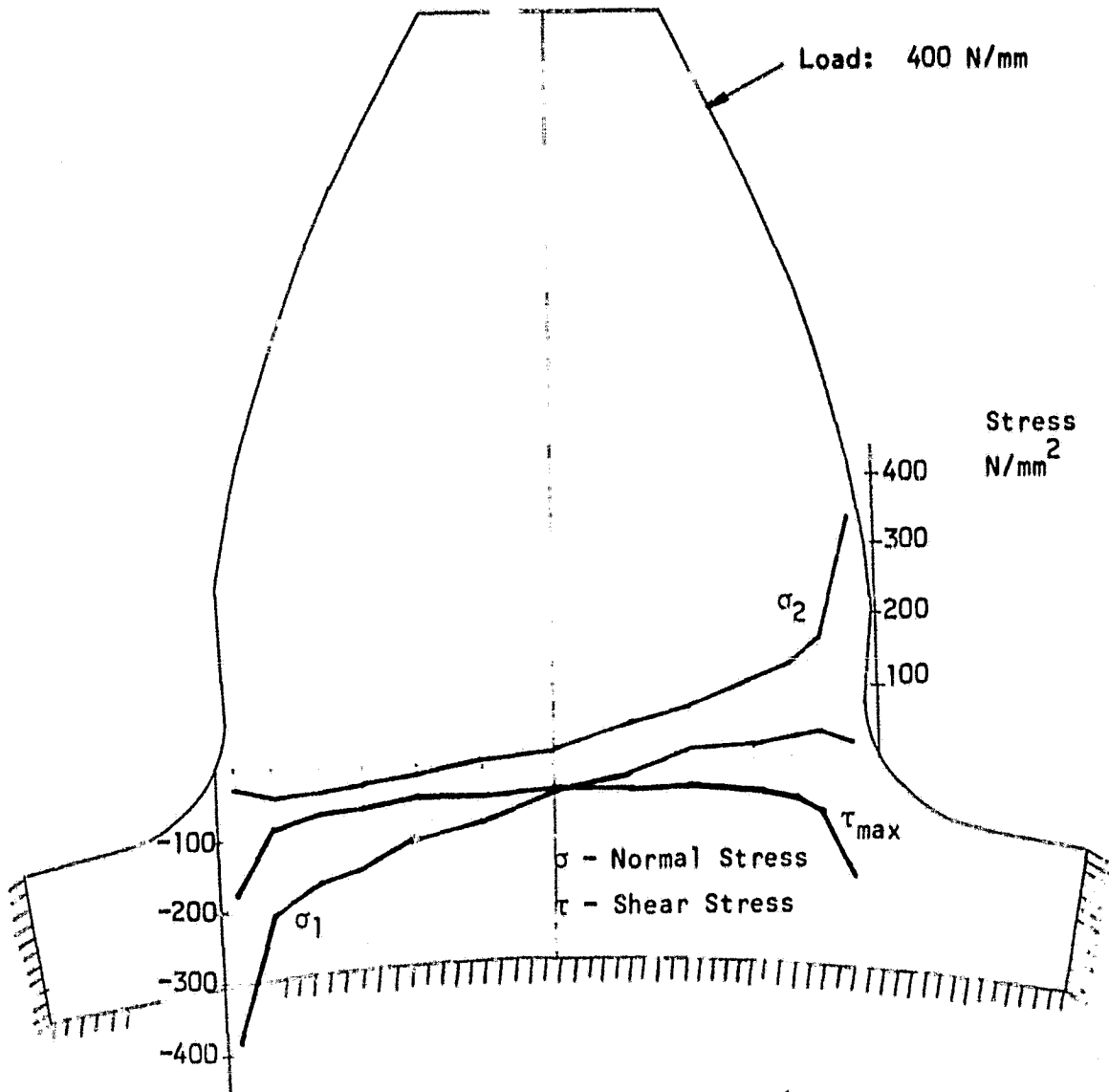


Figure 31. Internal Root Section Principal Stresses for a Fully Supported Rim with Near-Tip Loading with a Rim Radius of 37.1 mm.

ORIGINAL PAGE IS
OF POOR QUALITY

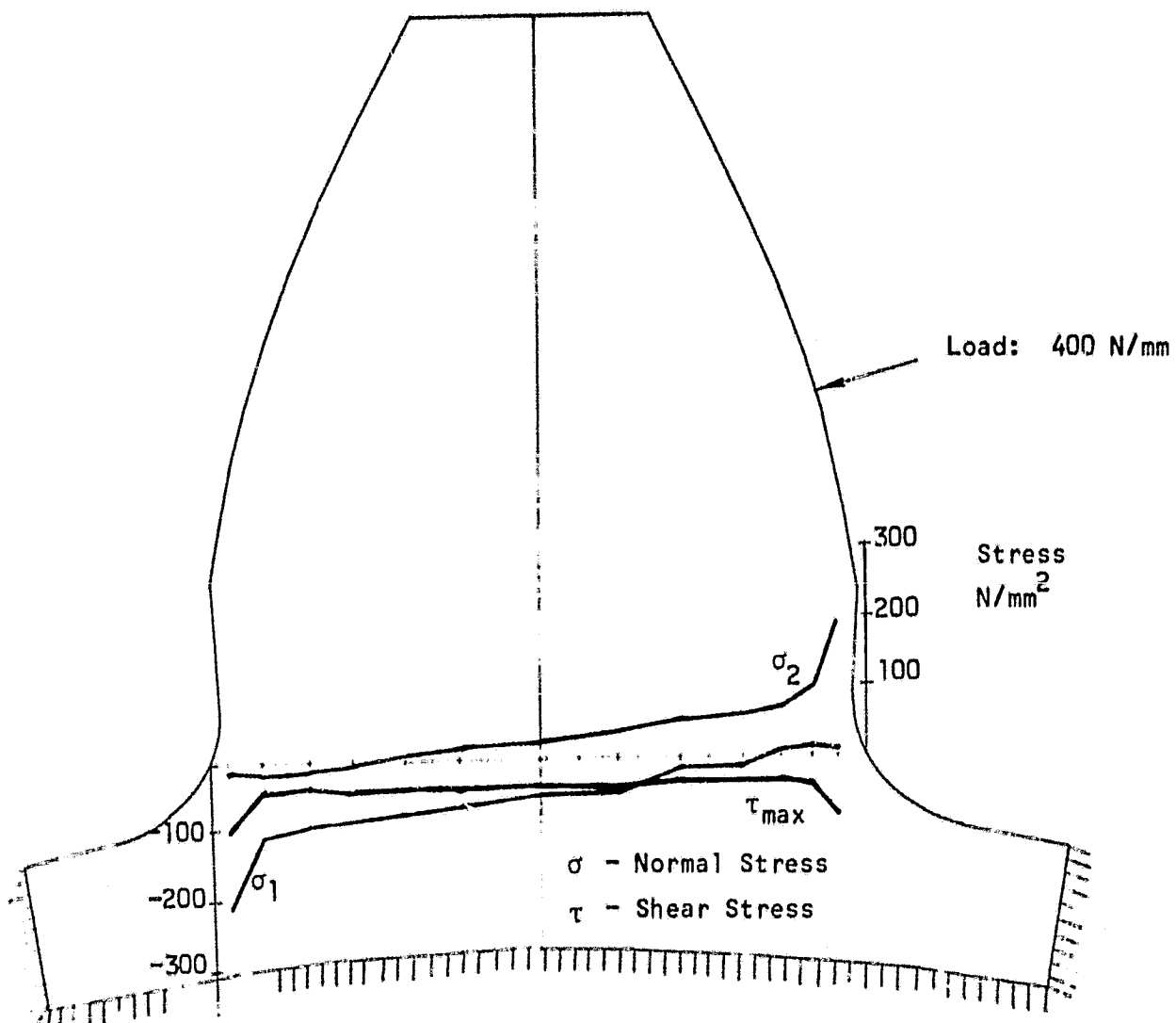


Figure 32. Internal Root Section Principal Stresses for a Fully Supported Rim with Pitch Point Loading with a Rim Radius of 37.1 mm.

ORIGINAL PAGE IS
OF POOR QUALITY

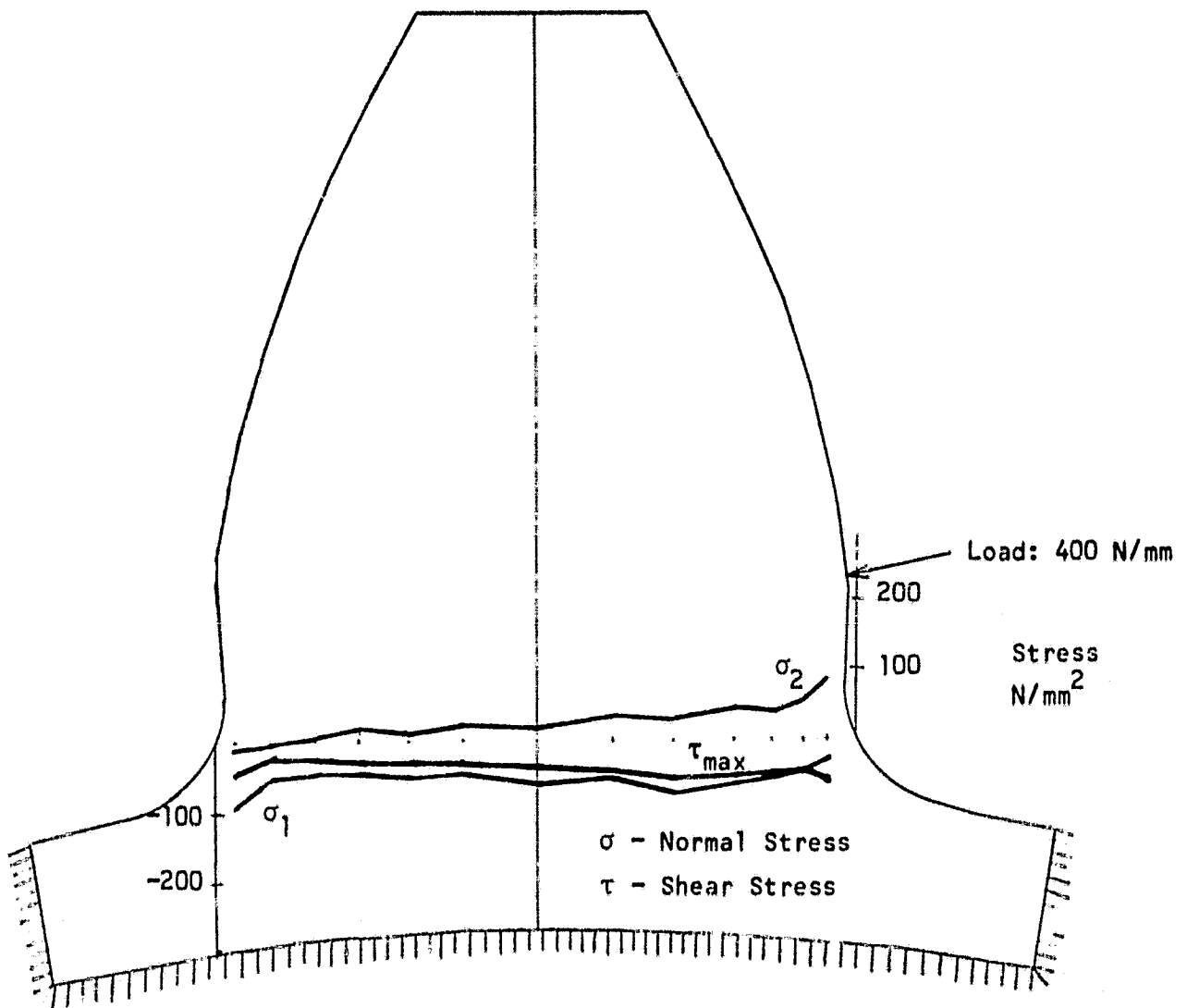


Figure 33. Internal Root Section Principal Stresses for a Fully Supported Rim with Near Root Loading with a Rim Radius of 37.1 mm.

ORIGINAL PAGE IS
OF POOR QUALITY

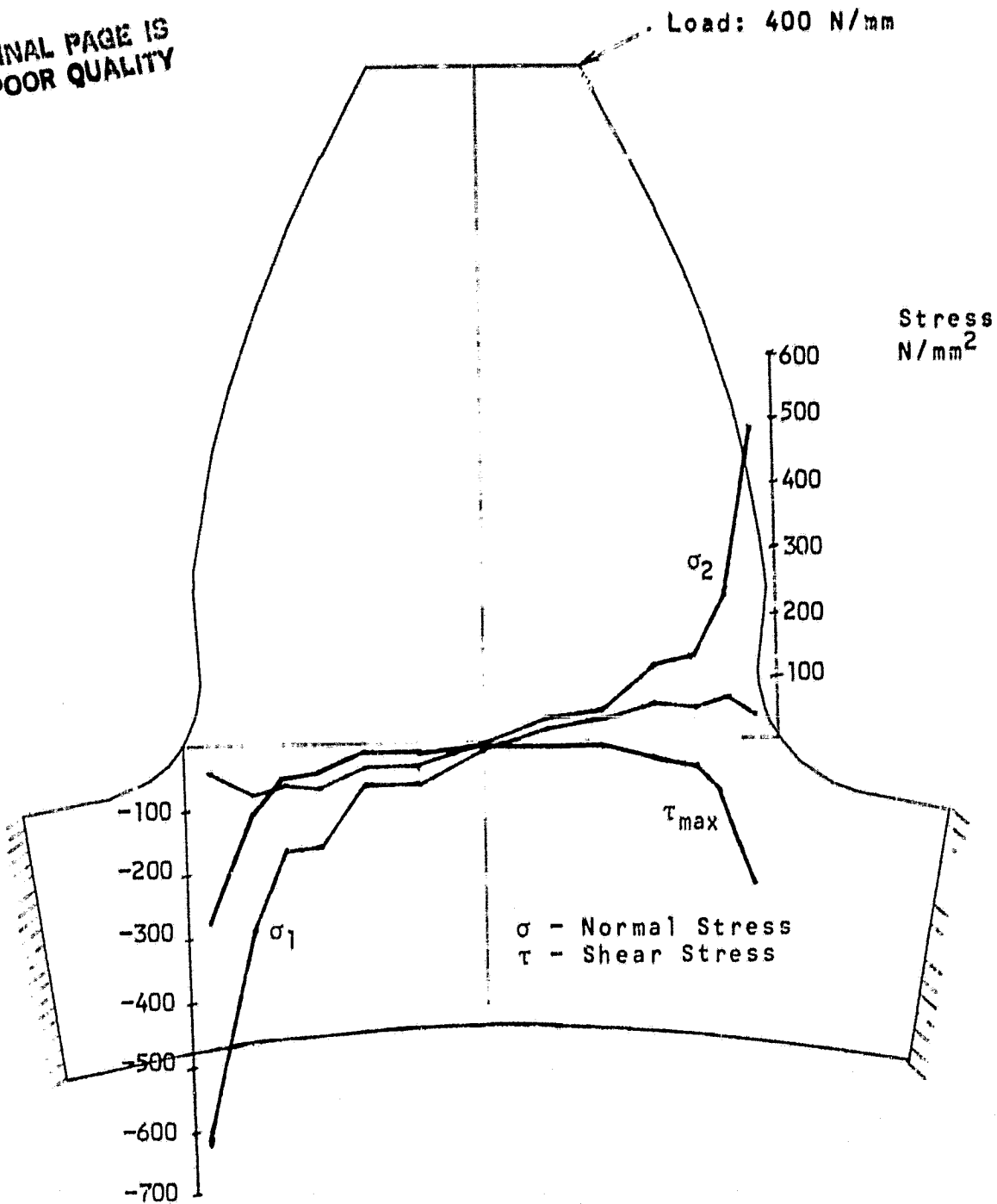


Figure 34. Internal Root Section Principal Stresses for a Partially Supported Rim with Tip Loading with a Rim Radius of 35 mm.

ORIGINAL PAGE IS
OF POOR QUALITY

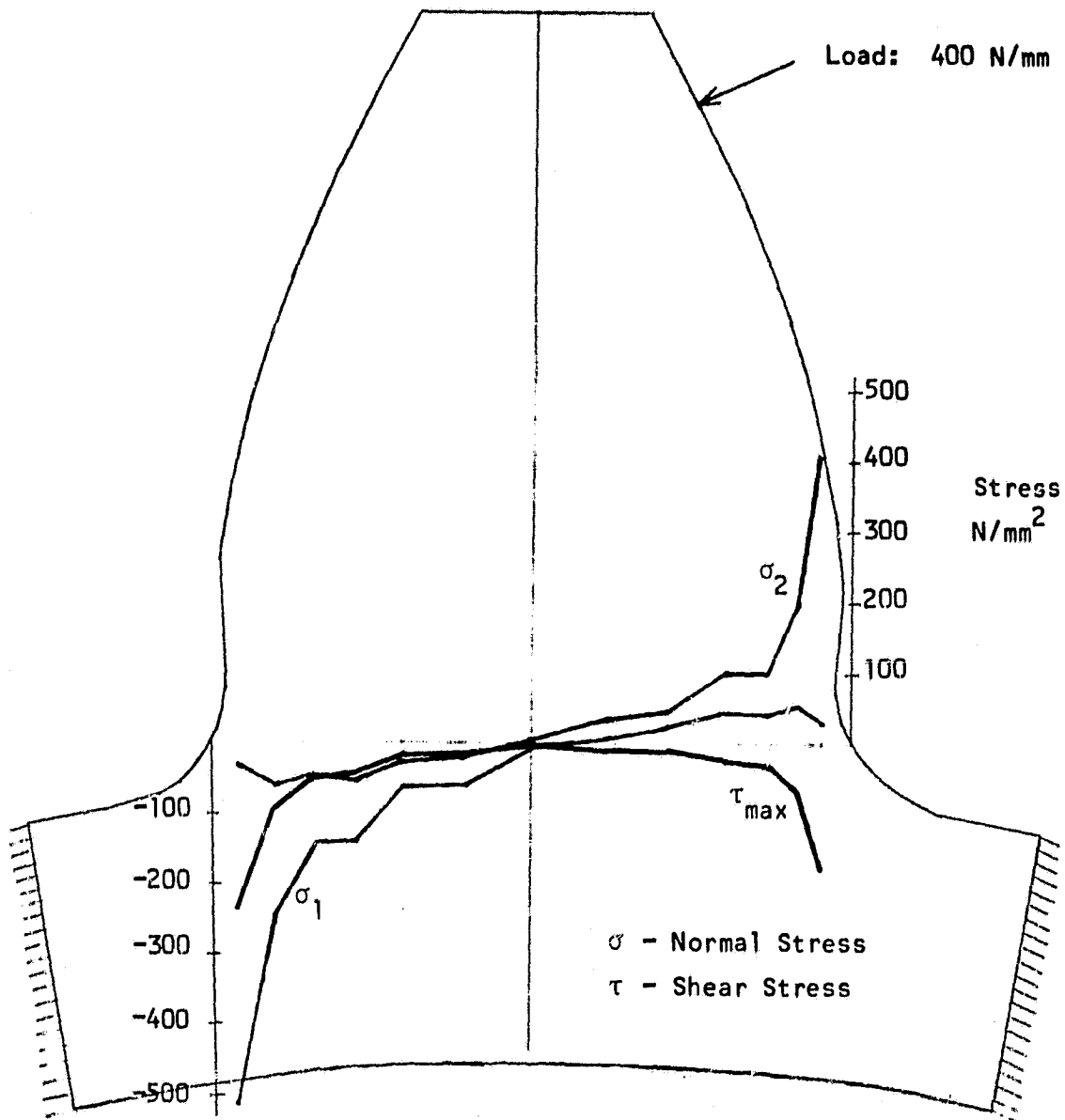


Figure 35. Internal Root Section Principal Stresses for a Partially Supported Rim with Near-Tip Loading with a Rim Radius of 35 mm.

ORIGINAL PAGE IS
OF POOR QUALITY

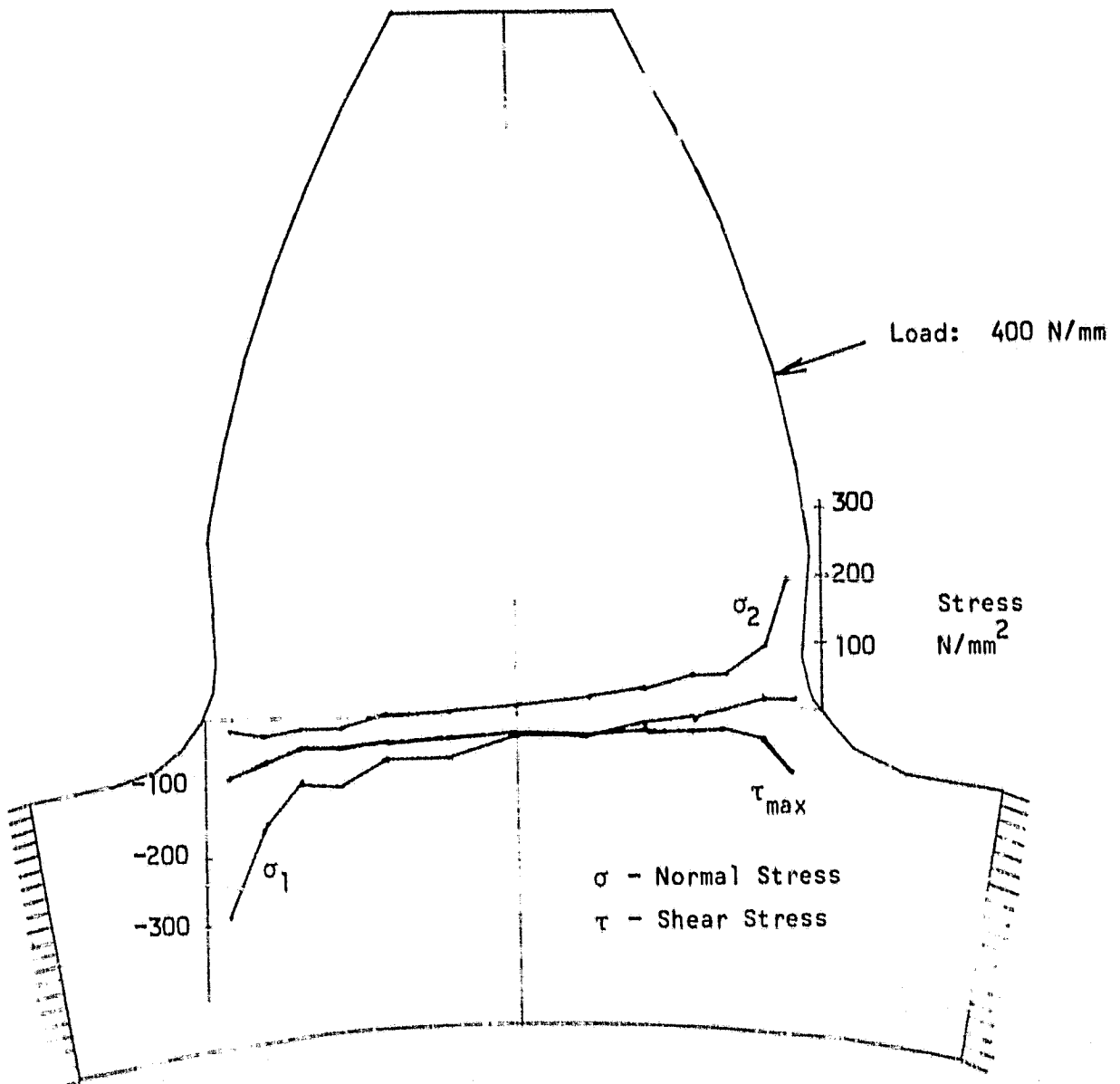


Figure 36. Internal Root Section Principal Stresses for a Partially Supported Rim with Pitch Point Loading with a Rim Radius of 35 mm.

ORIGINAL PAGE IS
OF POOR QUALITY

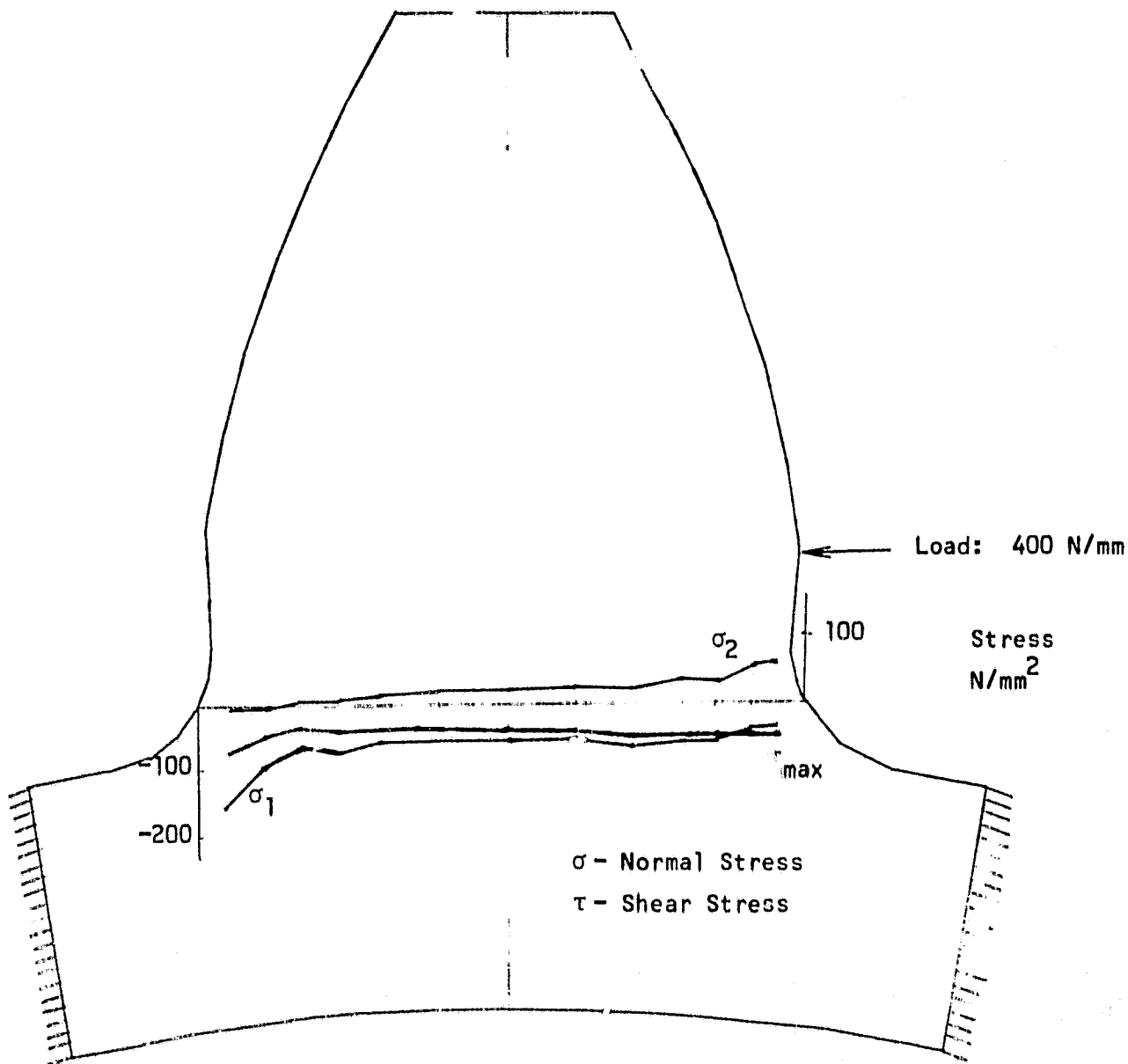


Figure 37. Internal Root Section Principal Stresses for a Partially Supported Rim with Near-Root Loading with a Rim Radius of 35 mm.

ORIGINAL PAGE IS
OF POOR QUALITY

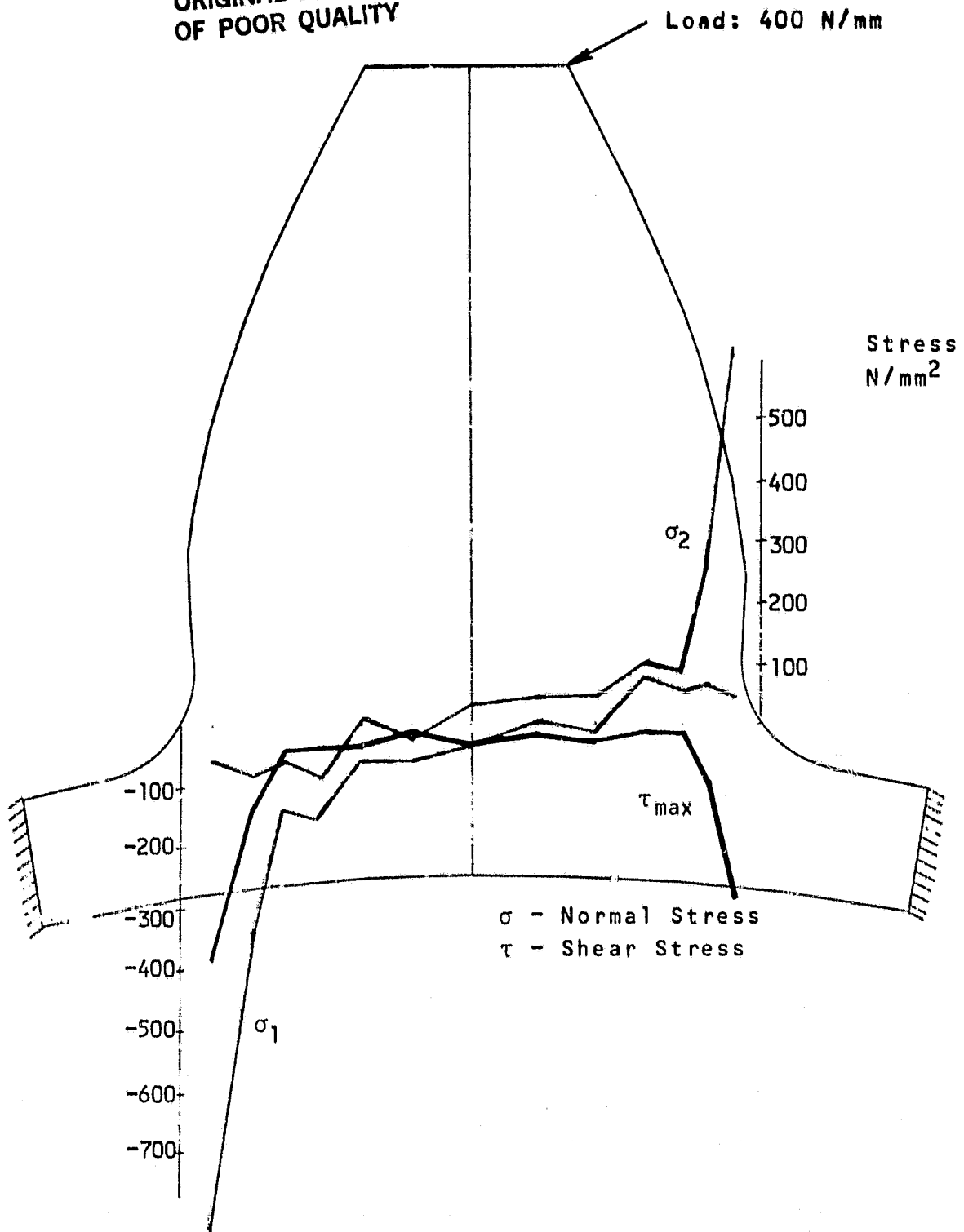


Figure 38. Internal Root Section Principal Stresses for a Partially Supported Rim with Tip Loading with a Rim Radius of 37.1 mm.

ORIGINAL PAGE IS
OF POOR QUALITY

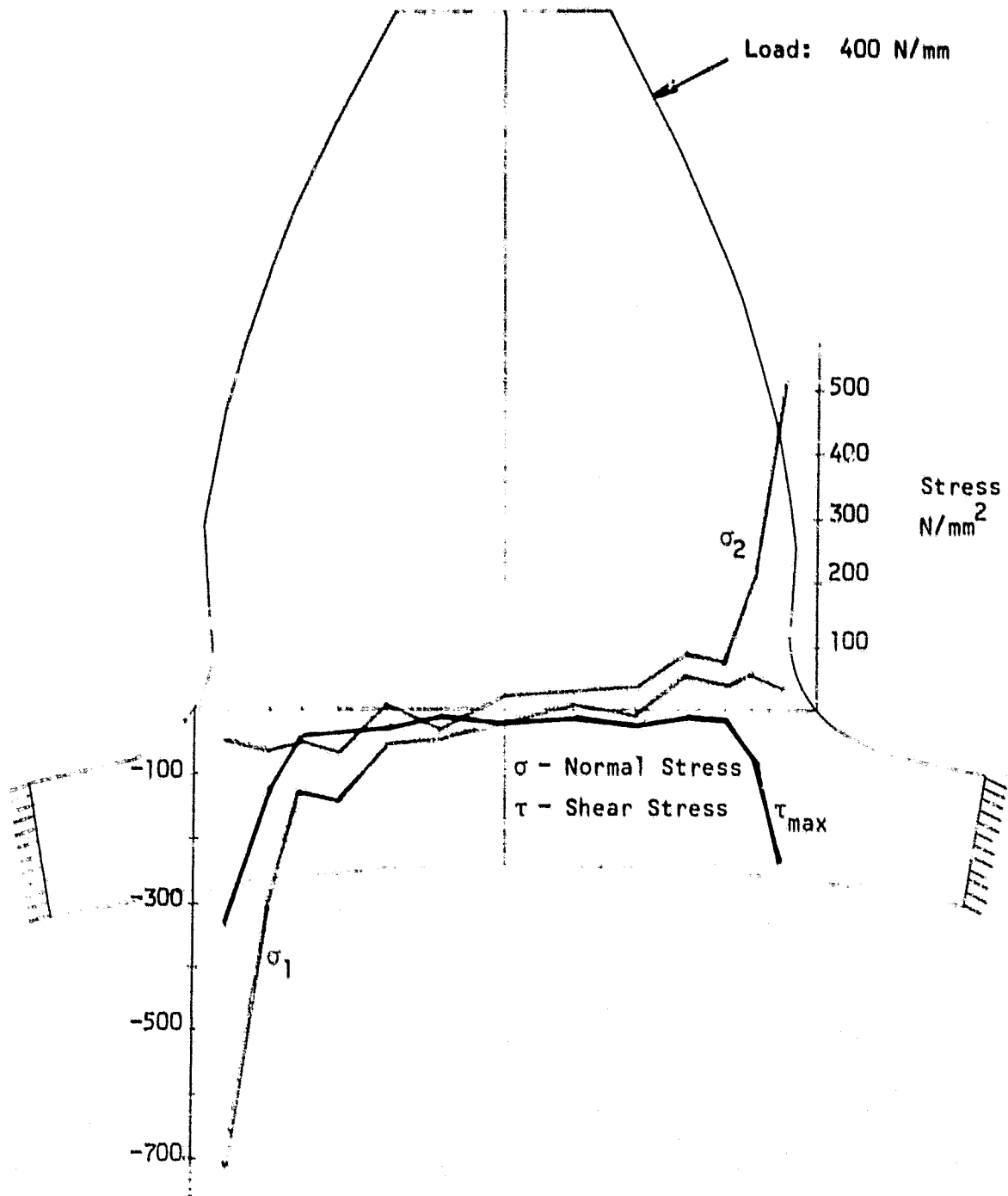


Figure 39. Internal Root Section Principal Stresses for a Partially Supported Rim with Near-Tip Loading with a Rim Radius of 37.1 mm.

ORIGINAL PAGE IS
OF POOR QUALITY

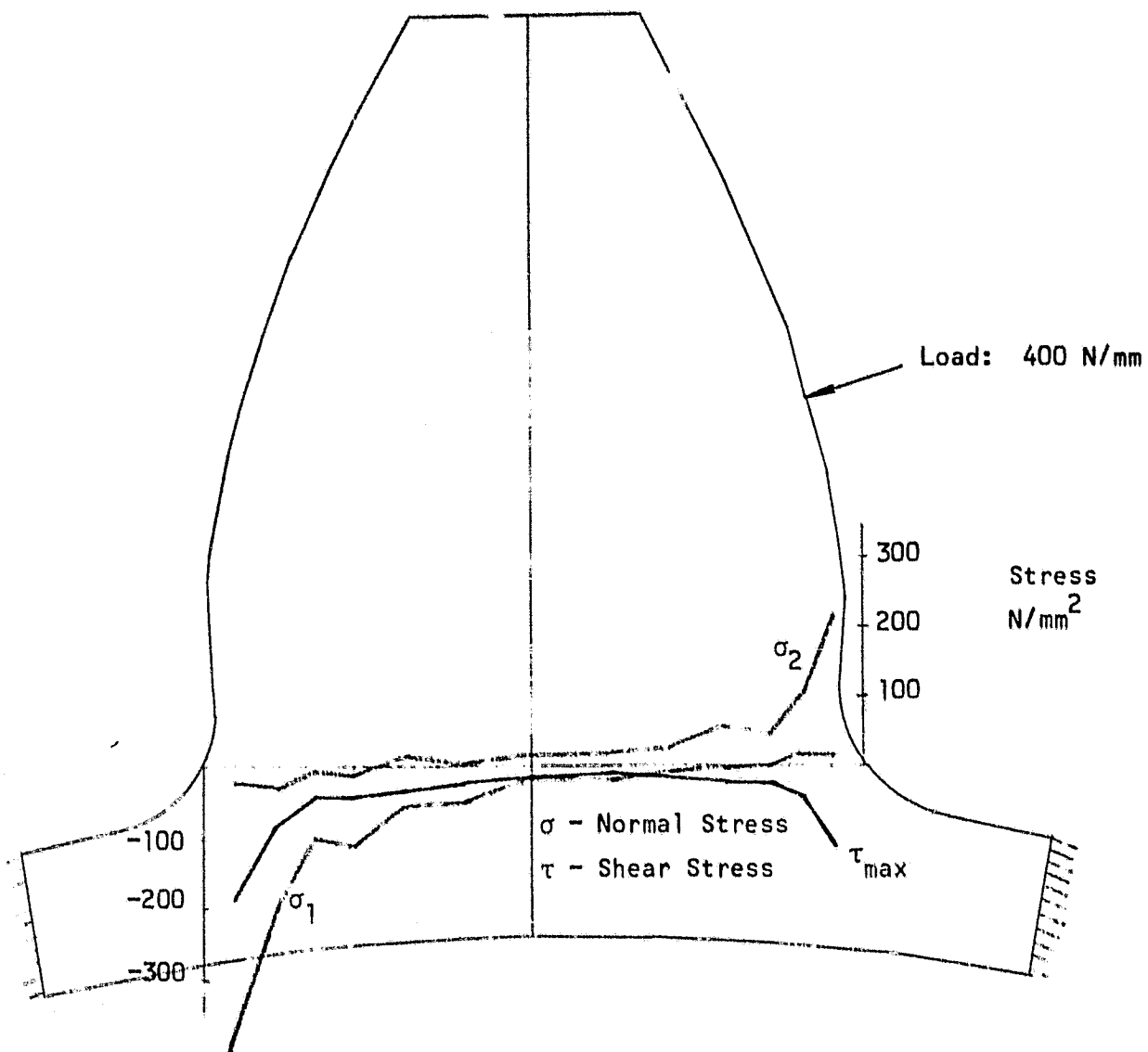


Figure 40. Internal Root Section Principal Stresses for a Partially Supported Rim with Pitch Point Loading with a Rim Radius of 37.1 mm.

ORIGINAL PAGE IS
OF POOR QUALITY

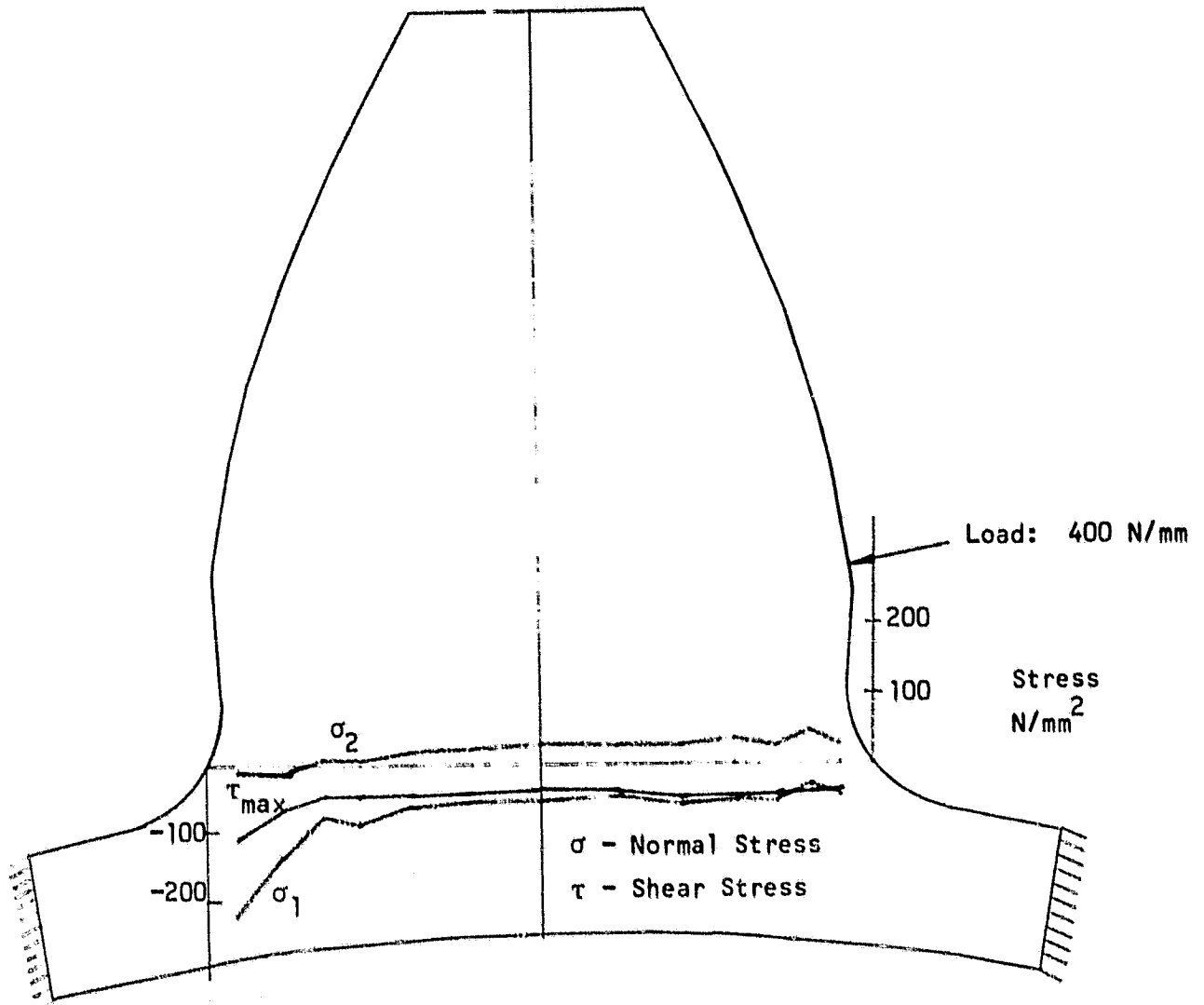


Figure 41. Internal Root Section Principal Stresses for a Partially Supported Rim with Near-Root Loading with a Rim Radius of 37.1 mm.

the rim thickness decreases. Moreover, for partially supported rims the compressive stresses, at the root opposite the loaded side increase at a greater rate than the tensile stresses at the root of the loaded side. These results are summarized graphically in Figure 25.

Finally, Figures 26. to 33. show the internal root section principal stresses for a fully supported rim with the same root radii and rim radii as above. The loading was at the points shown in Figure 3. and as shown in the figures with a magnitude of 400 N/mm as before. Similarly, Figures 34. to 41. show the internal root section principal stresses for a partially supported rim with the same root radii, rim radii, and loading. These results also show that the stresses decrease slightly with decreasing rim thickness for fully supported rims, but they increase with rim thickness for partially supported rims.

These results are consistent with recent experimental findings recorded by Drago and Lutthans.

ORIGINAL PAGE IS
OF POOR QUALITY

CONCLUSIONS

There are several results from this analysis which could be helpful to designers:

1. The rim thickness and rim support have a significant effect upon the stresses -- particularly for partially supported thin rims, with the compressive root stresses, opposite the loading side, being most affected. The stresses increase with decreasing rim thickness for partially supported rims (such as with loose-fitting hubs). However, for fully supported rims (such as with tight-fitting hubs) the stresses decrease slightly with decreasing rim thickness. For large rim thickness the rim support has little effect upon the stresses.
2. The maximum stresses occur at the root surfaces, except for local stress concentrations immediately beneath the load. These root stresses increase with decreasing fillet radii.
3. The fillet radius has very little effect upon the internal root section stresses.
4. The SAP-IV finite element method is a very effective procedure for investigating gear tooth stresses with a variety of loading, support, and geometrical shapes. The method can provide the benchmark analyses of gear tooth stresses, replacing many of the currently used handbook formulas.

REFERENCES

1. Bathe, K.-J., Wilson, E. L., and Peterson, F. E., "SAP-IV - A Structural Analysis Program for Static and Dynamic Response of Linear Systems," Earthquake Engineering Research Center, Report No. EERC 73-11, University of California, Berkeley, 1974.
2. Baronet, C. N., and Tordion, G. V., "Exact Stress Distribution in Standard Gear Teeth and Geometry Factors," Trans. ASME, Journal of Engineering for Industry, Vol. 95, 1973, pp. 1159-1163.
3. Cardou, A., and Tordion, G. V., "Numerical Implementation of Complex Potentials for Gear Tooth Stress Analysis," Trans. ASME, Journal of Mechanical Design, Vol. 103, 1981, pp. 461-465.
4. Chabert, G., Dang Tron, T., and Mathis, R., "An Evaluation of Stresses and Deflection of Spur Gear Teeth Under Strain," Trans ASME, Journal of Engineering for Industry, Vol. 96, 1974, pp. 85-93.
5. Chan, S. K., and Tuba, I. S., "A Finite Element Method for Contact Problems of Solid Bodies," International Journal of Mechanical Sciences, Vol. 13, 1971, pp. 615-625.
6. Cornell, R. W., "Compliance and Stress Sensitivity of Spur Gear Teeth," Trans ASME, Journal of Mechanical Design, Vol. 103, 1981, pp. 447-459.
7. Oda, S., Nagamura, K., and Aoki, K., "Stress Analysis of Thin Rim Spur Gears by Finite Element Method," Bulletin of the JSME, Vol. 24, No. 193, 1981, pp. 1273-1280.
8. Premilhat, A., Tordion, G. V., and Baronet, C. N., "An Improved Determination of the Elastic Compliance of a Spur Gear Tooth Acted on by a Concentrated Load," Trans. ASME, Journal of Engineering for Industry, Vol. 96, 1974, pp. 382-384.
9. Shotter, B. A., "A New Approach to Gear Tooth Root Stresses," Trans. ASME, Journal of Engineering for Industry, Vol. 96, 1974, pp. 11-18.
10. Tobe, T., Kato, M., and Inoue, K., "Bending of Stub Cantilever Plate and Some Applications to Strength of Gear Teeth," Trans. ASME, Journal of Mechanical Design, Vol. 100, 1978, pp. 374-381.

11. Tobe, T., Kato, M., and Inoue, K., "True Stresses and Stiffness of Spur Gear Teeth," Proceedings of the Fifth World Conference on Theory of Machines and Mechanisms, ASME, 1979, pp. 1105-1108.
12. Wilcox, L., and Coleman, W., "Application of Finite Elements to the Analysis of Gear Tooth Stresses," Trans. ASME, Journal of Engineering for Industry, Vol. 95, 1973, pp. 1139-1148.
13. Winter, H., and Hirt, M., "The Measurement of Actual Strains at Gear Teeth, Influence of Fillet Radius on Stresses and Tooth Strength," Trans. ASME, Journal of Engineering for Industry, Vol. 96, 1974, pp. 33-40.
14. Jacobson, M. A., "Bending Stresses in Spur Gear Teeth: Proposed New Design Factors Based on a Photo-Elastic Investigation," Proceedings, Institute of Mechanical Engineers, 169(31), 1955, pp. 587-609.
15. Aida, T., and Terauchi, Y., "On the Bending Stress of a Spur Gear," Bulletin JSME, Vol. 5, 1962, pp. 161-170.
16. Roark, R. J., and Young, W. C., Formulas for Stress and Strain, Fifth Edition, 1975, p. 187.
17. Drago, R. J., and Latthans, R. V., "An Experimental Investigation of the Combined Effects of Rim Thickness and Pitch Diameter on Spur Gear Tooth Root and Fillet Stresses," AGMA Paper No. P229.22, American Gear Manufacturers Association Fall Technical Meeting, Toronto, 1981.

ORIGINAL PAGE IS
OF POOR QUALITY